γ-ray spectroscopy of ^{191,193}Bi

P. Nieminen,[1] S. Juutinen,[1] A. N. Andreyev,[2,3] J. F. C. Cocks,[1] O. Dorvaux,[1,*] K. Eskola,[4] P. T. Greenlees,[1] K. Hauschild,[5,†] K. Helariutta,[1,‡] M. Huyse,[2] P. M. Jones,[1] R. Julin,[1] H. Kankaanpää,[1] H. Kettunen,[1] P. Kuusiniemi,[1] Y. Le Coz,[5] M. Leino,[1] T. Lönnroth,[6] M. Muikku,[1,§] P. Rahkila,[1] A. Savelius,[1] J. Uusitalo,[1] N. Amzal,[3] N. J. Hammond,[3,‖] C. Scholey,[3,1] and R. Wyss[7]

[1]*Department of Physics, P. O. Box 35 (YFL), FIN-40014 University of Jyväskylä, Finland*
[2]*Instituut voor Kern- en Stralingsfysica, K.U. Leuven, Leuven, Belgium*
[3]*Oliver Lodge Laboratory, University of Liverpool, Liverpool, United Kingdom*
[4]*Department of Physical Sciences, University of Helsinki, Helsinki, Finland*
[5]*DAPNIA/SPhN, CEA Saclay, France*
[6]*Department of Physics, Åbo Akademi, Turku, Finland*
[7]*Physics Department, The Royal Institute of Technology, Stockholm, Sweden*

(Received 2 December 2003; published 30 June 2004)

Prompt and delayed γ rays from ^{191,193}Bi have been identified using the recoil-decay tagging, isomer tagging, and recoil gating techniques, resulting in extensive level schemes for both nuclei. Excitation energies of the isomeric $13/2^+$ states have been established and oblate strongly coupled bands built on them have been observed. The nearly spherical $9/2^-$ ground-state bands appear to be crossed by more oblate-deformed low-lying structures. The properties of the bands feeding the $1/2^+$ intruder states indicate some structural change between ^{193}Bi and ^{191}Bi. The deformation associated with each of these states has been extracted from total Routhian surface calculations which also reveal the development of prolate minima with decreasing neutron number. $B(M1)/B(E2)$ ratios have been measured for the observed strongly coupled bands in order to resolve the intrinsic excitations. The observed quasiparticle structures in ^{193}Bi and high-spin isomers both in ^{193}Bi and ^{191}Bi are interpreted based on the coupling of the odd proton to the even-even Pb core.

DOI: 10.1103/PhysRevC.69.064326 PACS number(s): 21.10.−k, 23.20.Lv, 27.80.+w

I. INTRODUCTION

The bismuth ($Z=83$) nuclei lie in the lead region where there is a large amount of experimental evidence for various nuclear shapes coexisting at low excitation energies in the neutron-deficient Hg ($Z=80$), Tl ($Z=81$), Pb ($Z=82$), and Po ($Z=84$) isotopes [1,2]. The first observation of shape coexistence in this region was made in isotope shift measurements which revealed a shape transition in the ground states between the odd-A ^{187}Hg and ^{185}Hg [3,4]. Subsequently, the knowledge has been gained via α-decay fine-structure and β-decay studies as well as by γ-ray detection. The explanation for these structures can be derived from the intruder scenario, where the development of nonsphericity in neutron-deficient nuclei is associated with low-lying shell-model intruder states formed by exciting protons across the $Z=82$ shell gap [1,2]. Oblate-deformed structures are generally attributed to two-proton excitations whereas prolate deformation is associated with more complex configurations involving the elevation of four or more protons across the shell gap [2]. An alternative approach to account for the shape coexistence phenomenon is provided by the Nilsson model [5] where the energies of single-particle states are calculated in a deformed nuclear potential. These two models have been observed to be in good overall agreement, as demonstrated by Heyde *et al.* [6] for the lowest 0^+ intruder states in the neutron-deficient even-even Pb isotopes.

Recently, more information on these intruder states has been collected via the observation of associated γ-ray cascades in several successful in-beam experiments [7]. For example, when moving towards the neutron midshell, the yrast bands established in even-A Hg isotopes exhibit a weakly oblate shape until in ^{188}Hg, where a crossing with a well-deformed prolate band is observed [2]. The low-lying structures in the neutron-deficient lead isotopes are dominated by spherical states until competing oblate band structures appear close to $A=190$ (see Ref. [8] for ^{190}Pb, and references therein). In lighter isotopes, prolate-deformed rotational yrast bands have been observed in the even-A $^{188-182}$Pb (see Ref. [9] for ^{182}Pb, and references therein). Similarly, in polonium isotopes a prolate yrast intruder band in ^{190}Po with $N=106$ [10] and oblate structures a few neutrons away from the midshell have been established [11]. In thallium nuclei, the onset of prolate deformation is observed in ^{189}Tl and prolate-deformed bands are found to dominate the low-lying structure of the lighter odd-A isotopes (see Ref. [12], and references therein).

In accordance with the spherical shell model, the ground states of all neutron-deficient odd-A bismuth isotopes down

*Present address: Institut de Recherches Subatomique, CNRS-IN2P3, 23 Rue du Loess, BP 28, F-67037 Strasbourg, France.
†Present address: CSNSM, IN2P3-CNRS, F-91405 Orsay Cedex, France.
‡Present address: Laboratory of Radiochemistry, P. O. Box 55, FIN-00014 University of Helsinki, Finland.
§Present address: Radiation and Nuclear Safety Authority Finland, P. O. Box 14, FIN-00881 Helsinki, Finland.
‖Present address: Physics Division, Argonne National Laboratory, Argonne, Illinois 60439, USA.

to ^{187}Bi have been assigned a spin and parity of $I^{\pi}=9/2^{-}$ [13] from α- and β-decay studies. A $1/2^{+}$ intruder state, observed over the whole range of known neutron-deficient odd-A Bi isotopes is found to become lowered in excitation energy with decreasing neutron number [1,14–16]. This state is associated with a $2p$-$1h$ shell-model intruder configuration where a proton is elevated across the $Z=82$ shell thereby leaving a hole in the $s_{1/2}$ orbital [17]. An isomeric $13/2^{+}$ state has been identified in isotopes with $209 \leqslant A \leqslant 195$ [13] and recently in ^{189}Bi [18] and ^{187}Bi [19]. In the heavier isotopes down to ^{195}Bi, the lowest-lying quasiparticle states have been successfully interpreted as the odd proton coupled to the spherical even-even Pb core [20–24]. However, as deformed band structures have been well established in the Hg, Tl, Pb, and Po isotopes with $N \lesssim 110$, a transformation towards collectivity might be expected also in the light bismuth isotopes. In in-beam experiments for ^{189}Bi and ^{187}Bi, a rotational structure has been associated with the $13/2^{+}$ state in ^{189}Bi and also tentatively in the $N=104$ midshell nucleus ^{187}Bi [25]. In the present work, spectroscopy of both prompt and delayed γ rays from the $^{193}\mathrm{Bi}_{110}$ and $^{191}\mathrm{Bi}_{108}$ isotopes was performed resulting in extensive level schemes for both nuclei. Part of the results obtained have been reported in Refs. [26,27].

II. EXPERIMENTAL METHODS

The experiments were carried out at the Accelerator Laboratory of the University of Jyväskylä (JYFL) using ion beams delivered by the $K=130$ MeV cyclotron. A 350 μg/cm^2 thick ^{165}Ho target was bombarded with a ^{32}S beam at energies from 142 to 157 MeV (in the center of the target) in 5 MeV steps populating excited states in ^{193}Bi via the $4n$ fusion evaporation channel.

The nucleus ^{191}Bi was produced in the $^{142}\mathrm{Nd}(^{52}\mathrm{Cr},p2n)$ reaction. The 470 μg/cm^2 thick ^{142}Nd target (99.8% enrichment) was covered with a 10 μg/cm^2 thick layer of carbon and backed with a carbon layer of 50 μg/cm^2 thickness. The beam energy was 235 MeV in the center of the target.

In both experiments, prompt γ rays were observed with the Jurosphere II array which in its full composition holds 15 Eurogam Phase I- [28], five Nordball- [29], and seven TESSA-type [30] Compton suppressed Ge detectors. The absolute photopeak efficiency of the array at 1.3 MeV was measured to be $\sim$1.6% in the ^{193}Bi experiment with one detector missing and $\sim$1.4% in the ^{191}Bi experiment where three detectors were absent and strong background activities were present. The Eurogam detectors were installed at angles of 133.6° and 157.6° and the TESSA and Nordball detectors at angles of 63°, 79.0°, and 101.0° with respect to the beam direction. Absorbers, consisting of a 0.25 mm thick layer of tin and a 0.5 mm thick layer of copper were positioned in front of each detector to reduce the counting rate due to x rays. The fusion-evaporation residues recoiling out of the thin target were separated from the primary beam and fission fragments using the gas-filled recoil separator RITU [31].

At the focal plane, the separated recoils were implanted into a 300 μm thick 80 mm (horizontal) $\times$ 35 mm (vertical) Si detector which was also used to observe the subsequently emitted α particles. The silicon detector, divided into 16 strips and position sensitive in the vertical direction, exhibited an average position resolution of $\sim$450 μm in the ^{191}Bi experiment. Decay events were distinguished from the recoil implantations by requiring an anticoincidence with a signal from the multiwire proportional avalanche counter (MWPAC) [32], installed up stream from the Si detector. γ rays following the deexcitation of isomeric states were detected with three Nordball and two TESSA Compton suppressed Ge detectors in close geometry around the Si-detector chamber.

A signal from the silicon detector was required to trigger the data acquisition system. In addition to the timing, the energy and position of the interaction, together with the information obtained from the Ge and gas detectors within 32 μs were stored into the same event. Recoil identification was based on temporal and spatial correlations between the observed implantations and their characteristic α decays. Prompt and delayed γ rays were associated with the nucleus of interest according to the principles of the recoil-decay tagging (RDT) [33,34] method. The isomer tagging technique was used to correlate γ rays across isomeric states and recoil gating was employed in the examination of γ-γ coincidences. When the α-decay half-life was unsuitably long for the RDT method, the assignment of γ rays was based upon their measured excitation functions.

III. RESULTS

A. ^{193}Bi

The $9/2^{-}$ ground state in ^{193}Bi [$t_{1/2}=67(3)$ s [35]] has a total α-decay branch of only $b_{\alpha}=3.5(15)\%$ [35]. However, about 265 000 α decays **(**$E_{\alpha}=5899(5)$ keV [$I_{\alpha}=95.8(5)\%$], $E_{\alpha}=6174(5)$ keV [$I_{\alpha}=4.2(5)\%$] [13]**)** from this state were observed in 110 h of effective beam time. The $1/2^{+}$ intruder state in ^{193}Bi lies at an excitation energy of 307(7) keV [13] and has a total α-decay branch of $b_{\alpha}=90^{+10}_{-20}\%$ [35]. From this state, approximately 180 000 α decays [$E_{\alpha}=6475(5)$ keV [13], $t_{1/2}=3.2(6)$ s [35]] were detected. The total α-particle energy spectrum following the $^{32}\mathrm{S}+^{165}\mathrm{Ho}$ reactions is shown in Fig. 1 and it is dominated by the 5899 and 6475 keV peaks together with the ^{192}Bi doublet [6052(5), 6060(5) keV [13]]. A major part of the experiment was performed using an average beam current of 25 pnA which was the maximum allowed by the Ge singles counting rate. In order to allow clean recoil-α correlations, about 13 500 of the observed α particles from the $1/2^{+}$ intruder state were collected using an average beam current of 3 pnA at a beam energy of 152 MeV.

Approximately 80% of the ^{193}Bi recoil distribution was covered by the Si detector and the probability to observe the α decay with its full energy was assumed to be 50%. A transmission of 20% was used for the RITU separator and the effect of the deterioration of the target observed during the experiment was also estimated. Taking into account the α-decay branching ratios, a cross section of about 3 mb for the $^{165}\mathrm{Ho}(^{32}\mathrm{S},4n)^{193}$Bi reaction at 152 MeV can be deduced.

Prior to the present work, no γ rays belonging to ^{193}Bi were known. Due to the long α-decay half-life of the $9/2^{-}$

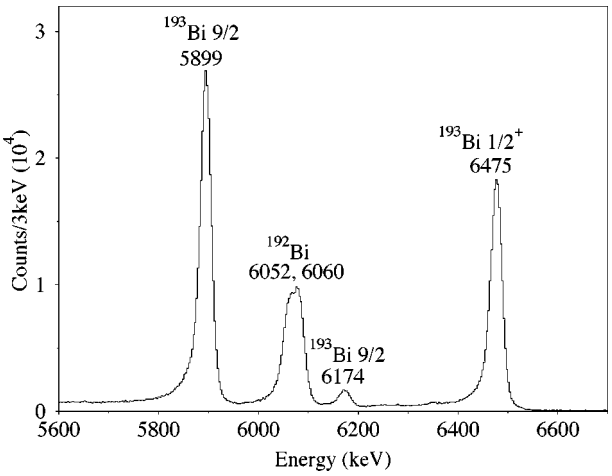

FIG. 1. Total energy spectrum of α particles observed in the focal-plane Si detector from $^{32}S+^{165}Ho\rightarrow^{197}Bi^*$ reactions at beam energies of 142, 147, 152, and 157 MeV. The gas counter signal was used as a veto.

ground state, the use of correlation methods to identify γ rays feeding this state was not possible. However, an isomeric $13/2^+$ state is known in odd-A bismuth isotopes down to $A=195$. This state lies at an excitation energy of 1196 and 888 keV in ^{197}Bi [21] and ^{195}Bi [20], respectively, and deexcites via an $M2$ γ-ray transition to the $9/2^-$ ground state. Lönnroth *et al.* [20] predict the excitation energy of the $13/2^+$ state in ^{193}Bi to be 460(50) keV which would correspond to a half-life of 0.5 μs. Their estimate of the lowering of the excitation energy of this state is based on the interaction of the $i_{13/2}$ proton with the increasing number of $i_{13/2}$ neutron holes as the $\nu i_{13/2}$ orbital opens up at $A=197$ and becomes more depleted in going to lighter isotopes.

The total spectrum of recoil-gated singles γ rays observed in the focal-plane Ge detectors up to 30 μs after the implantation of a recoil is shown in Fig. 2(a). There are several previously unknown lines in the energy range from 400 to 650 keV and the identification of the $13/2^+\rightarrow9/2^-$ transition from this spectrum alone is not possible. As the predicted half-life for the $13/2^+$ state is much shorter than the 30-μs time window, a spectrum of delayed γ rays observed within 220 ns after a recoil implantation was generated and is shown in Fig. 2(b). To create this spectrum, the data collected at a beam energy of 147 MeV were chosen as they have the best statistics. The effect of the shorter time window is to enhance the observed intensity of γ rays following the deexcitation of short-lived isomeric states relative to those depopulating isomers with longer halflives.

However, in the spectrum shown in Fig. 2(b) there are no candidates for the $13/2^+\rightarrow9/2^-$ transition in the predicted energy range of 400 to 500 keV while several unknown lines appear in the range of 500 to 650 keV. The 605 keV peak is much more prominent compared to other transitions than in the case of the longer time window [Fig. 2(a)], thus indicating a relatively short half-life. The half-life associated with each of these transitions is deduced from the distribution of time differences between the implantation of a recoil into the Si detector and the observation of the γ-ray of interest. The

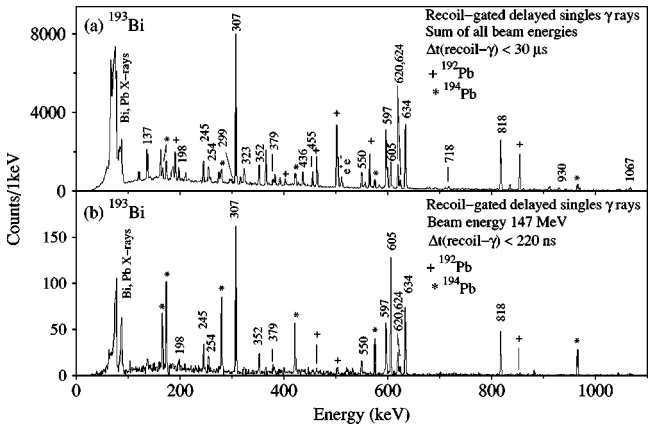

FIG. 2. Energy spectra of recoil-gated singles γ rays from $^{32}S+^{165}Ho$ reactions observed at the focal plane within (a) 30 μs and (b) 220 ns after the implantation of a recoil. In (a), a sum of spectra obtained at all beam energies is shown, in (b) a beam energy of 147 MeV was used. Transitions assigned to ^{193}Bi are marked with their energy, those belonging to ^{192}Pb and ^{194}Pb are indicated with plus signs and asterisks, respectively.

550, 597, 620, 624, and 634 keV transitions exhibit halflives of $t_{1/2}\gtrsim3$ μs which are far too long to agree with the prediction for the $13/2^+\rightarrow9/2^-$ transition. Moreover, they are in coincidence with each other and thus excluded from the presumed single-step deexcitation of the $13/2^+$ state. On the other hand, the half-life of 153(10) ns associated with the 605 keV transition [Fig. 3(a)] is closer to the prediction given for the $13/2^+$ state in ^{193}Bi. The Weisskopf estimate for the strength of this transition was calculated assuming that the deexcitation of a level at 605 keV proceeds only via the 605 keV γ ray. The obtained value of $B(M2)=0.062(10)$ W.u. is in very good agreement with that for the predicted transition energy of 460 keV with a half-life of 0.5 μs [$B(M2)\sim0.06$ W.u.]. The corresponding hindrance factor of 16 is of the same order of magnitude than the value of $\sim$45 for the $13/2^+\rightarrow9/2^-$ spin-flip transition in ^{197}At [36]. Therefore, the 605 keV transition is a strong candidate for the $13/2^+\rightarrow9/2^-$ transition in ^{193}Bi.

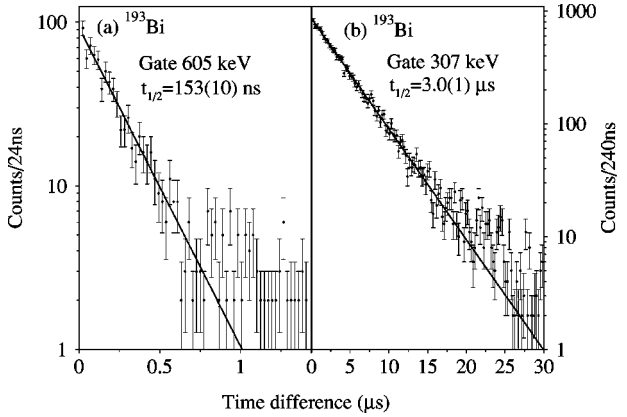

FIG. 3. Spectrum of time differences between the implantation of a recoil and the observation of a (a) 605 keV and (b) 307 keV γ ray in the focal-plane Ge detectors.

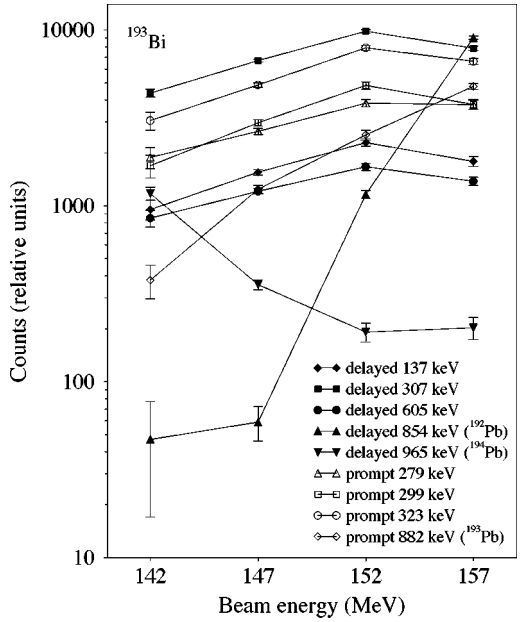

FIG. 4. Relative intensities of the 137, 307, and 605 keV delayed (filled symbols) and 279, 299, and 323 keV prompt (open symbols) γ rays as a function of beam energy normalized to the number of observed α decays of the $9/2^-$ state in ^{193}Bi. For comparison, intensities of the delayed 854 (^{192}Pb) and 965 keV (^{194}Pb) transitions together with the prompt 882 keV (^{193}Pb) γ ray are also shown.

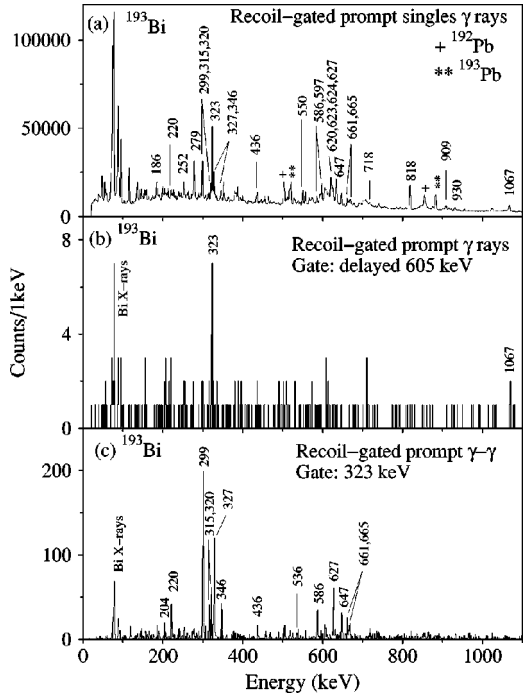

FIG. 5. (a) Recoil-gated singles spectrum of prompt γ rays from ^{32}S + ^{165}Ho reactions where transitions assigned to ^{193}Bi are marked with their energy. (b) Energy spectrum of recoil-gated prompt γ rays gated by the 605 keV delayed transition. (c) Recoil-gated spectrum of prompt γ rays gated by the 323 keV prompt transition.

To confirm the assignment of γ rays to ^{193}Bi, excitation functions were measured. The intensities of the observed γ rays were normalized to the number of detected α decays of the $9/2^-$ ground state at each of the beam energies. The resulting excitation function curves for selected delayed (137, 307, and 605 keV) and also prompt (279, 299, and 323 keV) γ rays are illustrated in Fig. 4. As is evident, the intensities of these transitions follow a consistent trend which is clearly different from the behavior of the corresponding curves for the 854 (^{192}Pb), 882 (^{193}Pb), and 965 keV (^{194}Pb) [13] transitions. Therefore, all these γ rays are associated with ^{193}Bi. The assignment of the 605 keV transition as deexciting the $13/2^+$ isomeric state in ^{193}Bi is also affirmed by these results.

The energy spectrum of recoil-gated prompt singles γ rays is presented in Fig. 5(a). In order to select the γ-ray transitions feeding the $13/2^+$ isomeric state in ^{193}Bi, a recoil-gated delayed-prompt γ-γ matrix was created. In this matrix, a gate set on the delayed 605 keV transition provides a spectrum of correlated prompt γ rays with a clear peak at 323 keV, as shown in Fig. 5(b). The low statistics in this spectrum is due to the short half-life of the $13/2^+$ state (153 ns) compared to the flight time of the ^{193}Bi recoils through the RITU separator ($\sim$1 μs). The 323 keV transition, also appearing in the recoil-gated singles γ-ray spectrum [Fig. 5(a)] is placed directly feeding the $13/2^+$ isomeric state. The coincident prompt γ rays were studied by analyzing a recoil-gated γ-γ matrix using the RADWARE software package [37]. A sample coincidence spectrum gated by the prompt 323 keV transition is illustrated in Fig. 5(c) showing two groups of transitions, one at $\sim$300 keV and the other at $\sim$600 keV which usually suggest the observation of a strongly coupled band. The deduced band structure feeding the $13/2^+$ state (band 1) is shown in the level scheme of ^{193}Bi (Fig. 6) and the assignment of two of the band members (323 and 299 keV) to ^{193}Bi is further confirmed by their measured excitation functions (Fig. 4).

Angular distributions for γ rays were determined from their observed intensities in recoil-gated spectra which were measured at a beam energy of 147 MeV with detectors at angles of 158° and 79° with respect to the beam direction. The extracted efficiency-corrected intensity ratios $R_{\mathrm{exp}} = I(158°)/I(79°)$, energies and intensities of γ rays, together with the properties of the energy levels in ^{193}Bi, are listed in Table I. For the band feeding the $13/2^+$ state, the obtained values of R_{exp} agree well with its suggested strongly coupled nature. The 323, 299, 327, 320, 346, and 315 keV transitions are assigned to be dipoles, probably $M1$ in character and the same assignment is tentatively made also for the 220 and 204 keV transitions although their low intensities do not permit angular distribution measurements. The R_{exp} values for the 647, 665, and 661 keV transitions are comparable with that of 1.43(10) for the 882 keV $17/2^+ \rightarrow 13/2^+$ $E2$ transition in ^{193}Pb and they are assigned to have quadrupole character. Their placement as crossover transitions in the band feeding the $13/2^+$ state yields $E2$ multipolarity for these three γ rays. The $E2$ assignment has also been made to the 623 and 627 keV transitions despite the lack of angular distribution information due to strong contamination from nearby lines, and for the 536 keV transition which is too weak for meaningful angular distribution measurements. The

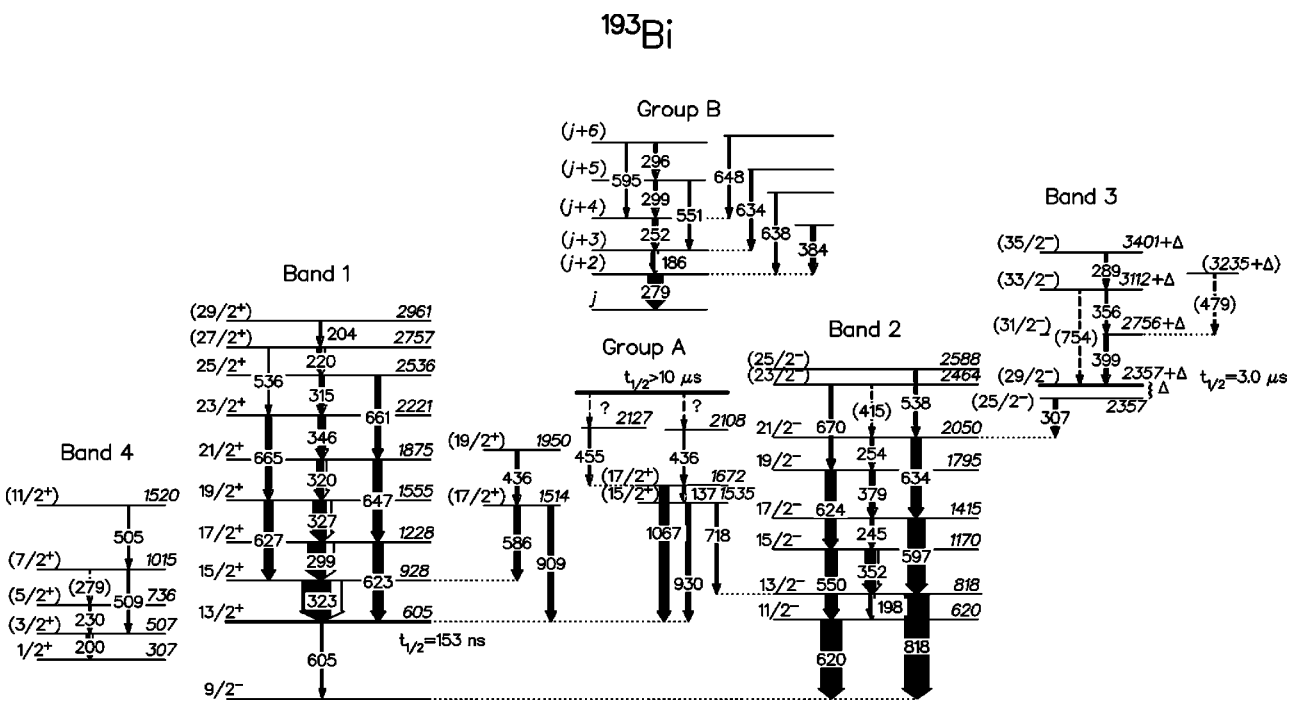

FIG. 6. Level scheme of ^{193}Bi.

586 keV transition is observed to be in coincidence with the 323 keV $15/2^+ \rightarrow 13/2^+$ transition [Fig. 5(c)] and assigned to be of dipole character indicating a $(17/2^+)$ state at 1514 keV. The 436 keV dipole transition is placed to feed this 1514 keV level and the coincident 909 keV transition to deexcite it and populate the $13/2^+$ band head.

As presented in Fig. 4, the measured excitation functions confirm the assignment of the 307 keV γ ray to ^{193}Bi. Figure 7(a) shows a spectrum generated by summing coincidences with the 307, 597, 634, and 818 keV transitions in a recoil-gated delayed γ-γ matrix. Due to intensity arguments, the 307 keV transition is placed to be the topmost in a cascade populated by the deexcitation of an isomeric state with an apparent half-life of 3.0(1) μs [see Fig. 3(b)]. As illustrated in Fig. 7(b), the same cascade of γ rays is observed also in the target-position array which indicates prompt feeding into the band and enables the determination of angular distributions as defined above. The negative-parity band (band 2) in the level scheme shown in Fig. 6 is constructed based on γ-γ coincidences of both prompt and delayed γ rays and placed to feed the $9/2^-$ ground state. The angular distributions R_{exp} suggest quadrupole character for the 818, 634, 550, and 307 keV transitions for which the $E2$ multipolarity is again more probable. Although the values of R_{exp} for the 597, 620, and 624 keV transitions could not be extracted, they are also assigned an $E2$ character, resulting in a spin and parity of $I^\pi=(25/2^-)$ for the state at 2357 keV. The 198, 352, 245, 379, and 254 keV γ rays are measured to have dipole character and given the assigned $E2$ character of the cross-over transitions, they most likely have $M1$ multipolarity. On the basis of weak coincidences, the 670 and 538 keV transitions observed in the gated spectrum of prompt γ rays [Fig. 7(b)] are placed to feed the $19/2^-$ and $21/2^-$ levels at 1795 and 2050 keV, respectively.

The presence of the 307 keV line in the spectrum of prompt γ rays gated by other strong transitions in the cascade [Fig. 7(b)] implies that the microsecond isomer lies above the 2357 keV level and that the deexciting transitions from this state remain unobserved. This nonobservation is most probably due to the very low energy of these transitions, closely resembling the deexcitation of the 12^+ isomeric state in the ^{192}Pb core [38]. This suggested coupling of the $h_{9/2}$ proton to the 12^+ core state could yield a spin and parity of $I^\pi=(29/2^-)$ for the isomeric state in ^{193}Bi, in accordance with the observed $29/2^-$ isomeric states in the heavier odd-A bismuth isotopes [13]. In order to study γ rays feeding the $(29/2^-)$ state, a spectrum of prompt γ rays gated by the delayed 307 keV transition was generated and is shown in Fig. 7(c). The 399, 356, and 289 keV lines are tentatively assigned to be $M1$ in character and placed to feed the isomeric level at $2357+\Delta$ keV (band 3 in Fig. 6).

The energy spectrum of delayed γ rays gated by the 137 keV transition is shown in Fig. 7(d) and the deduced irregular level structure is illustrated in Fig. 6 (group A). The assignment of these transitions to ^{193}Bi is based on the measured excitation function for the 137 keV transition (Fig. 4). The 1067 keV transition is present in the spectrum of recoil-gated prompt singles γ rays [Fig. 5(a)] and also in the spectrum of prompt γ rays gated by the delayed 605 keV $13/2^+ \rightarrow 9/2^-$ transition [Fig. 5(b)]. Consequently, the 1067 keV γ ray is placed to feed the $13/2^+$ isomeric state and assigned to have an $E2$ character based on the measured angular distributions. The 436 and 455 keV transitions are in coincidence with the 1067 keV transition in both prompt and delayed γ-γ matrices and placed parallel to each other feeding the $(17/2^+)$ state at 1672 keV. Inspection of the delayed γ-γ matrix reveals the presence of a 137 keV self-coincident doublet [Fig. 7(d)]. On the basis of coincidences and energy

TABLE I. Energies (E_γ), intensities (I_γ), and angular distributions $R_{\mathrm{exp}}=I(158°)/I(79°)$ of γ rays in ^{193}Bi. The energies of initial states (E_i) and spins and parities of initial (I_i^π) and final (I_f^π) levels are also given.

E_γ (keV)	I_γ (%)	E_i (keV)	I_i^π	I_f^π	$R_{\mathrm{exp}}=I(158°)/I(79°)$
137.0(5)	1.8(6)	1672	$(17/2^+)$	$(15/2^+)$	
185.7(5)	7.7(10)		$(j+3)$	$(j+2)$	
198.0(5)	7.3(6)	818	$13/2^-$	$11/2^-$	0.9(2)
199.9(5)	9.0(5)	507	$(3/2^+)$	$1/2^+$	1.0(3)
204(1)	3.0(5)	2961	$(29/2^+)$	$(27/2^+)$	
220(1)	12.7(5)	2757	$(27/2^+)$	$25/2^+$	
229.5(5)	2.3(10)	736	$(5/2^+)$	$(3/2^+)$	
245.2(5)	6.4(8)	1415	$17/2^-$	$15/2^-$	0.8(2)
252.3(5)	10.4(10)		$(j+4)$	$(j+3)$	0.7(2)
254.0(5)	5.5(6)	2050	$21/2^-$	$19/2^-$	0.7(4)
278.8(3)	45(1)		$(j+2)$	j	1.15(7)
279.2(5)	1.7(6)	1015	$(7/2^+)$	$(5/2^+)$	
289.2(5)	4.1(6)	$3401+\Delta$	$(35/2^-)$	$(33/2^-)$	0.6(3)
295.7(5)	5.5(7)		$(j+6)$	$(j+5)$	
298.8(5)	5.5(8)		$(j+5)$	$(j+4)$	
299.3(5)	61(4)	1228	$17/2^+$	$15/2^+$	0.82(7)
307.0(5)	10.5(9)	2357	$(25/2^-)$	$21/2^-$	1.2(2)
315.2(5)	11.4(8)	2536	$25/2^+$	$23/2^+$	0.71(15)
319.9(5)	23.6(14)	1875	$21/2^+$	$19/2^+$	0.74(8)
323.4(3)	100(6)	928	$15/2^+$	$13/2^+$	0.90(6)
327.3(3)	47(3)	1555	$19/2^+$	$17/2^+$	0.84(7)
345.8(5)	18.6(11)	2221	$23/2^+$	$21/2^+$	0.67(11)
351.9(3)	36(3)	1170	$15/2^-$	$13/2^-$	0.86(9)
355.3(7)	1.8(7)				
356(1)	5.2(11)	$3112+\Delta$	$(33/2^-)$	$(31/2^-)$	0.6(3)
379.3(5)	13.6(14)	1795	$19/2^-$	$17/2^-$	0.71(14)
384(1)	10.9(13)			$(j+2)$	
398.8(5)	9.0(5)	$2756+\Delta$	$(31/2^-)$	$(29/2^-)$	0.8(2)
415.2(5)	2.3(6)	2464	$(23/2^-)$	$21/2^-$	
432(1)	2.9(9)				
436.0(5)	9(2)	1950	$(19/2^+)$	$(17/2^+)$	0.92(11)
436(1)	3.1(12)	2108		$(17/2^+)$	
455.0(5)	3.6(14)	2127		$(17/2^+)$	
458.5(7)	1.8(7)				
468.8(7)	2.4(8)				
479(1)	6.0(13)	$(3235+\Delta)$		$(31/2^-)$	
504.5(5)	4.3(7)	1520	$(11/2^+)$	$(7/2^+)$	
508.9(5)	5.0(16)	1015	$(7/2^+)$	$(3/2^+)$	
536(1)	2.7(8)	2757	$(27/2^+)$	$23/2^+$	
538(1)	9.1(8)	2588	$(25/2^-)$	$21/2^-$	
550.0(3)	37(3)	1170	$15/2^-$	$11/2^-$	1.30(10)
551.1(5)	6.1(9)		$(j+5)$	$(j+3)$	
585.9(5)	19(3)	1514	$(17/2^+)$	$15/2^+$	1.0(2)
595(1)	1.5(8)		$(j+6)$	$(j+4)$	
597.0(3)	56(4)	1415	$17/2^-$	$13/2^-$	
605.0(5)		605	$13/2^+$	$9/2^-$	
620.0(5)	68(1)	620	$11/2^-$	$9/2^-$	

TABLE I. (*Continued.*)

E_γ (keV)	I_γ (%)	E_i (keV)	I_i^π	I_f^π	$R_{\exp}=I(158°)/I(79°)$
622.7(5)	32(3)	1228	$17/2^+$	$13/2^+$	
624.5(5)	34(3)	1795	$19/2^-$	$15/2^-$	
626.6(5)	29(3)	1555	$19/2^+$	$15/2^+$	
634.4(5)	34(3)	2050	$21/2^-$	$17/2^-$	1.17(8)
634(1)	8.2(11)			$(j+3)$	
638(1)	5.5(13)			$(j+2)$	
647.1(5)	26(2)	1875	$21/2^+$	$17/2^+$	1.54(11)
648(1)	4.5(9)			$(j+4)$	
661.2(5)	18.6(11)	2536	$25/2^+$	$21/2^+$	1.36(11)
665.2(5)	15.9(12)	2221	$23/2^+$	$19/2^+$	1.46(14)
670.0(5)	12.3(12)	2464	$(23/2^-)$	$19/2^-$	1.5(2)
718.5(5)	8.6(14)	1535	$(15/2^+)$	$13/2^-$	
754(1)	4.5(5)	$3112+\Delta$	$(33/2^-)$	$(29/2^-)$	
818.2(3)	85(9)	818	$13/2^-$	$9/2^-$	1.34(7)
909.2(9)	20(9)	1514	$(17/2^+)$	$13/2^+$	1.2(2)
930.0(5)	14.5(15)	1535	$(15/2^+)$	$13/2^+$	1.0(2)
1067(1)	29.5(13)	1672	$(17/2^+)$	$13/2^+$	1.50(11)

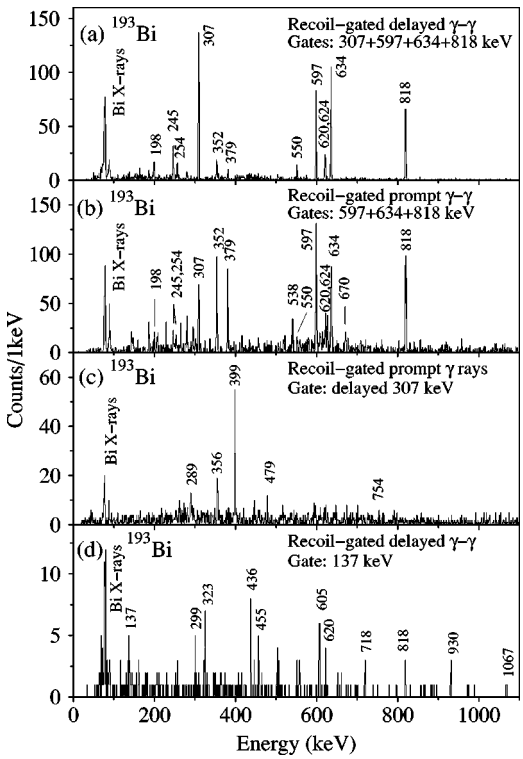

FIG. 7. Energy spectra of recoil-gated γ rays from the ^{32}S + ^{165}Ho reactions. (a) Sum of spectra of delayed γ rays gated by the delayed 307, 597, 634, and 818 keV transitions. (b) Sum of spectra of prompt γ rays gated by the prompt 597, 634, and 818 keV transitions. (c) Spectrum of prompt γ rays gated by the 307 keV delayed transition. (d) Spectrum of delayed γ rays gated by the delayed 137 keV transition.

sum arguments, one component of the 137 keV doublet together with the 930 keV transition is placed in the level scheme parallel to the 1067 keV transition. As the self-coincidence of the 137 keV transition or its coincidence with the 1067 keV transition are not observed in the prompt γ-γ matrix, it is likely that the second 137 keV component forms part of the fragmented deexcitation path from the long-lived isomer. The 718 keV transition is placed as a connecting transition to band 2 from which the low-lying 620 and 818 keV transitions also appear in Fig. 7(d). The 299 and 323 keV transitions present in this spectrum indicate feeding to band 1 based on the $13/2^+$ state but discrete links could not be established. The half-life of the isomer is too long to be accurately measured in the present experiment where the time window for the observation of delayed γ rays after the implantation of a recoil is limited to 32 μs. The measured distribution of time differences suggests a lower limit of $\sim$10 μs for the half-life associated with the 137 keV transition.

The 279 keV transition which is clearly observed in the spectrum of recoil-gated prompt singles γ rays [Fig. 5(a)] is firmly assigned to ^{193}Bi based on its measured excitation function (Fig. 4). The analysis of the prompt γ-γ matrix revealed transitions with energies of 186, 252, 296, 299, 384, 551, 595, 634, 638, and 648 keV which are all associated with ^{193}Bi. Angular distribution measurements imply quadrupole character for the 279 keV transition while values of $R_{\exp}$ for the other members of the group could not be extracted due to overlapping strong lines. The link between this group (group B in Fig. 6) and the rest of the level scheme could not be established from the present data, most probably due to isomeric character of the band head (spin j in Fig. 6). If this assumption is correct, the boundary conditions of the present experimental system would restrict its half-life to a range of 20 ns$\lesssim t_{1/2} \lesssim$150 ns.

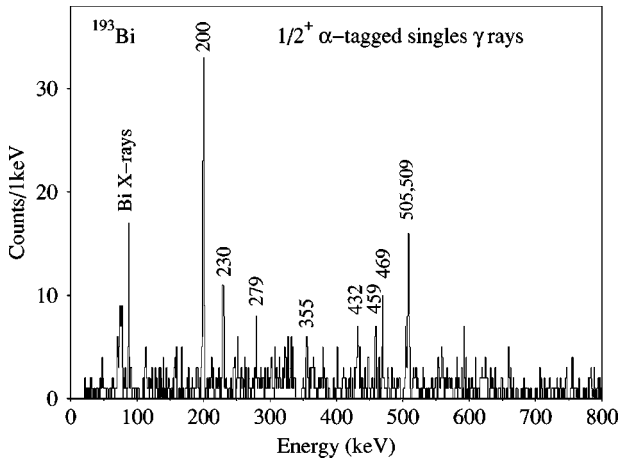

FIG. 8. Energy spectrum of prompt singles γ rays gated by recoils and tagged with the 6475 keV α decay of the $1/2^+$ intruder state in ^{193}Bi.

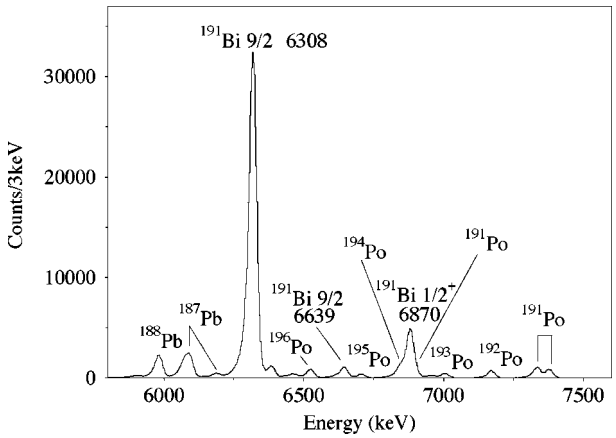

FIG. 9. Energy spectrum of α particles observed in the focal-plane Si detector from the ^{52}Cr+^{142}Nd reactions. The gas counter veto is present. The Po isotopes with $A \geqslant 193$ are produced in reactions with heavier Nd isotopes contaminating the target.

Prompt γ rays feeding the $1/2^+$ intruder state in ^{193}Bi were studied using the data collected at low beam current. The spectrum of singles γ rays gated by recoils and tagged with the 6475 keV α decay of the $1/2^+$ state using a search time of 9 s is displayed in Fig. 8. The 200 keV transition, which is isotropic according to angular distribution measurements, is tentatively assigned to be of $M1$ character and placed to directly feed the $1/2^+$ state. The 230, (279), 505, and 509 keV transitions are placed into the level scheme (band 4 in Fig. 6) on the basis of weak coincidence relations and energy sum arguments, whereas the location of the observed 355, 432, 459, and 469 keV transitions could not be resolved.

B. ^{191}Bi

In about 130 h of effective beam time, the two α-decay branches from the $9/2^-$ ground state in ^{191}Bi (E_α=6308(3) keV [14] [I_α=97.1(3)%] [13], E_α =6639(5) keV [13] [I_α=2.9(3)%] [13]) yielded approximately 380 000 full-energy events in the singles α-particle energy spectrum shown in Fig. 9. The Po isotopes with $A \geqslant 193$ are produced in the fusion of the ^{52}Cr beam with heavier Nd isotopes contaminating the target. The $9/2^-$ state has a half-life of $t_{1/2}$=12.4(4) s [14] and a total α-decay branch of b_α=51(10)% [14]. From the $1/2^+$ intruder state [b_α=68(5)% [14]] lying at an excitation energy of 242 keV [13], about 65 000 α decays [E_α=6870(3) keV, $t_{1/2}$ $=121^{+8}_{-7}$ ms [14]] were observed. The approximate average beam current was 12 pnA. A cross section of $\sim$150 μb was extracted for the ^{142}Nd(^{52}Cr,$p2n$)^{191}Bi reaction at 235 MeV by adopting the same detection and transmission efficiencies as in the ^{193}Bi experiment and taking into account the Si-detector coverage of about 70% of the ^{191}Bi recoil distribution.

Following the systematics for the excitation energy of the isomeric $13/2^+$ state with decreasing N, it would be expected to lie at approximately 400 keV in ^{191}Bi. Assuming a similar deexcitation path and transition strength than in ^{193}Bi, the decrease in excitation energy would correspond to a longer half-life for this state and the deexciting $13/2^+ \rightarrow 9/2^-$ $M2$ transition is likely to be observed in the focal-plane Ge detectors.

The energy spectrum of delayed γ rays gated by recoils and tagged with the α decay of the $9/2^-$ ground state using a search time of 13 s is shown in Fig. 10. Despite the long α-decay half-life, the resulting spectrum is clean containing a very strong peak at an energy of 430 keV together with a few weaker lines. The half-life associated with the 430 keV transition was measured to be $t_{1/2}$=562(10) ns from the distribution of time differences between the recoil implantation and the observation of a 430 keV γ ray in the focal-plane Ge detectors (see the inset of Fig. 10). The corresponding transition strength was calculated assuming that a level at 430 keV deexcites only via the 430 keV transition. The resulting value of $B(M2)$=0.073(5) W.u. is comparable with that of the $13/2^+ \rightarrow 9/2^-$ transition in ^{193}Bi [$B(M2)$

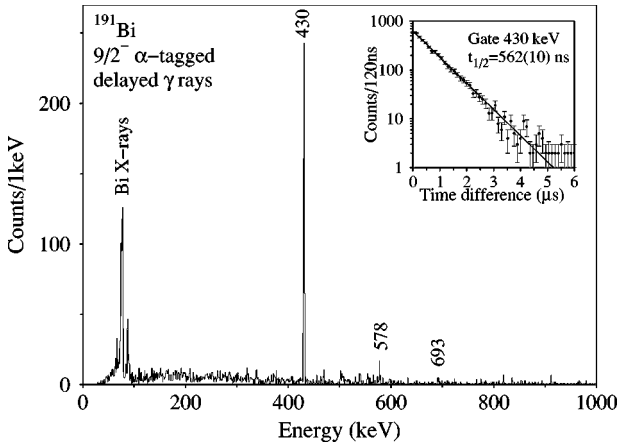

FIG. 10. Energy spectrum of recoil-gated delayed γ rays tagged with the α decay of the $9/2^-$ ground state in ^{191}Bi. In the inset, spectrum of time differences between the implantation of a recoil and the observation of a 430 keV γ ray in the focal-plane Ge detectors is presented.

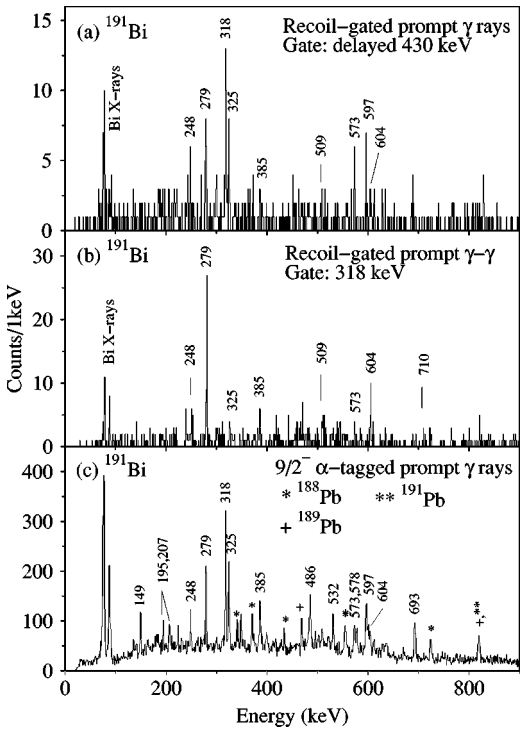

FIG. 11. (a) Energy spectrum of recoil-gated prompt γ rays from the ^{52}Cr+^{142}Nd reactions gated by the 430 keV delayed transition. (b) Spectrum of recoil-gated prompt γ rays gated by the 318 keV transition. (c) Spectrum of prompt γ rays gated by recoils and tagged with the 6308 keV α decay of the $9/2^-$ ground state in ^{191}Bi. The identified peaks from background activities are marked with their nucleus of origin.

$=0.062(10)$ W.u.]. Moreover, the observed intensity of bismuth K x rays can be accounted for only if $M2$ character is assumed for the 430 keV γ ray. Excluding the weak lines in the spectrum, the observed γ-ray and bismuth K x-ray intensities yield a conversion coefficient of $\alpha_K=0.61\pm0.10$ for the 430 keV transition while calculations for the two lowest multipoles give $\alpha_K(E1)=0.013$, $\alpha_K(E2)=0.030$, $\alpha_K(M1)=0.15$, and $\alpha_K(M2)=0.44$ [39]. Therefore, the 430 keV transition is firmly assigned to be the $13/2^+\rightarrow9/2^-$ transition in ^{191}Bi.

In order to examine prompt γ rays feeding the $13/2^+$ isomeric state in ^{191}Bi, a recoil-gated delayed-prompt γ-γ matrix was generated and the isomer tagging method was applied to the 430 keV transition. The resulting spectrum of prompt γ rays is illustrated in Fig. 11(a) showing an arrangement of transitions into two groups as in the coincidence spectrum for ^{193}Bi [Fig. 5(c)], again clearly indicating the observation of a strongly coupled band. The 318 keV transition is placed to feed directly the $13/2^+$ isomeric state as it is the most intense peak in the spectrum and similar in energy to the 323 keV $15/2^+\rightarrow13/2^+$ transition in ^{193}Bi. The rest of the band feeding the $13/2^+$ level (band 1 in Fig. 12) was constructed from an analysis of a recoil-gated prompt γ-γ matrix, from which a sample coincidence spectrum gated by the 318 keV transition is presented in Fig. 11(b).

Angular distributions for the observed γ rays were extracted as the intensity ratio $R_{exp}=I(134°,158°)/I(79°,101°)$ in spectra of recoil-gated γ rays. The obtained values are listed in Table II along with energies and intensities of γ rays and the properties of the energy levels in ^{191}Bi. The results support dipole character for the 318, 279, 325, and 248 keV transitions belonging to the strongly coupled band. An $M1$ assignment for these four γ rays is again more probable. The angular distribution measurements also indicate quadrupole character for the 573 keV transition, whereas values of R_{exp} for the 597 and 604 keV γ rays could not be extracted due to the many overlapping lines close to 600 keV. However, these three transitions are assigned to be of $E2$ multipolarity based on their crossover character within the band. The 385 keV dipole transition tentatively defining a $(21/2^+)$ level at 1736 keV, the 710 keV transition linking this state to the $17/2^+$ state of band 1 and the 509 keV γ ray all are placed in the level scheme based on γ-γ coincidences.

A spectrum of recoil-gated prompt γ rays tagged with the α decay of the $9/2^-$ ground state using a search time of 13 s is presented in Fig. 11(c). As the recoil rate in the Si detector was high relative to the half-life of 12.4 s of this state, an unambiguous identification of γ rays directly feeding the $9/2^-$ ground state in ^{191}Bi from this spectrum is not possible. However, the 578 and 693 keV transitions are present also in the spectrum of delayed γ rays (Fig. 10) and assigned to ^{191}Bi. These two transitions, together with γ rays having energies of 486, 207, 532, 325, and (599) keV are placed in a band feeding the $9/2^-$ ground state (band 2 in Fig. 12). Angular distribution measurements indicate dipole and quadrupole character for the 486 and 693 keV transitions, respectively, while the R_{exp} ratios for the other band members could not be determined. This negative-parity structure resembles the band feeding the $9/2^-$ ground state in ^{193}Bi, including an isomeric state for which a half-life of $t_{1/2}=400(40)$ ns is extracted using the time differences between the recoil implantation and observation of a 578 keV γ ray. However, the

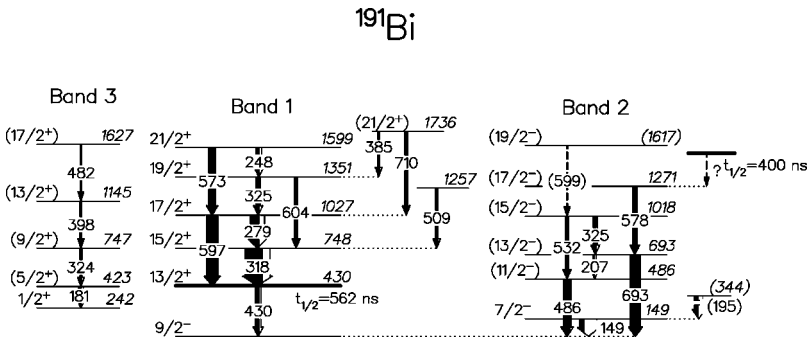

FIG. 12. Level scheme of ^{191}Bi.

TABLE II. Energies (E_γ), intensities (I_γ), and angular distributions $R_{\rm exp}=I(134°,158°)/I(79°,101°)$ of γ rays in ^{191}Bi. The energies of initial states (E_i) and spins and parities of initial (I_i^π) and final (I_f^π) levels are also given.

E_γ (keV)	I_γ (%)	E_i (keV)	I_i^π	I_f^π	$R_{\rm exp}=$ $I(134°,158°)/$ $I(79°,101°)$
149.0(5)	22(3)	149	$7/2^-$	$9/2^-$	0.91(12)
180.9(7)	17(3)	423	$(5/2^+)$	$1/2^+$	0.9(2)
187.0(7)	6(2)				
194.7(7)	18(5)	(344)		$7/2^-$	0.8(2)
207.1(7)	7(4)	693	$(13/2^-)$	$(11/2^-)$	
248.2(7)	17(5)	1599	$21/2^+$	$19/2^+$	0.8(2)
278.6(5)	50(5)	1027	$17/2^+$	$15/2^+$	0.76(8)
297.2(7)	3(1)				
318.3(5)	100(10)	748	$15/2^+$	$13/2^+$	0.78(7)
324.2(7)	11(3)	747	$(9/2^+)$	$(5/2^+)$	
324.6(7)	17(9)	1018	$(15/2^-)$	$(13/2^-)$	
324.8(5)	19(7)	1351	$19/2^+$	$17/2^+$	0.81(8)
344.0(7)	3(1)				
368.6(7)	5(2)				
385(1)	10(5)	1736	$(21/2^+)$	$19/2^+$	0.92(9)
397.6(7)	9(3)	1145	$(13/2^+)$	$(9/2^+)$	
429.7(5)		430	$13/2^+$	$9/2^-$	
459(1)	3(1)				
482(1)	6(2)	1627	$(17/2^+)$	$(13/2^+)$	
486.0(5)	39(6)	486	$(11/2^-)$	$9/2^-$	0.7(2)
509(1)	14(7)	1257		$15/2^+$	
527(1)	3(1)				
532(1)	20(6)	1018	$(15/2^-)$	$(11/2^-)$	
544(1)	3(1)				
553(1)	3(1)				
572.8(7)	38(11)	1599	$21/2^+$	$17/2^+$	1.1(2)
578.0(7)	29(5)	1271	$(17/2^-)$	$(13/2^-)$	1.9(4)
597.0(7)	63(10)	1027	$17/2^+$	$13/2^+$	
599.1(7)	8(4)	(1617)	$(19/2^-)$	$(15/2^-)$	
603.7(7)	20(6)	1351	$19/2^+$	$15/2^+$	
693.1(7)	55(8)	693	$(13/2^-)$	$9/2^-$	1.1(2)
710(1)	17(8)	1736	$(21/2^+)$	$17/2^+$	

direct deexcitation of the isomeric state is not observed and prompt γ rays feeding this state can not be resolved as the population intensity is weak and the half-life is short compared to the flight time of the ^{191}Bi recoils through the RITU separator.

The 149 keV transition [Fig. 11(c)] is found to follow the α decay of the mother nucleus ^{195}At and placed to directly feed the $9/2^-$ ground state in ^{191}Bi [14]. In that work, the 149 keV transition is determined to be of $M1$ multipolarity which indicates negative parity and a spin value of 7/2, 9/2, or 11/2 for the initial state. As no transition between the $13/2^+$ state at 430 keV and the 149 keV level was observed, a spin of 7/2 for this state could be deduced. The 195 keV transition [see Fig. 11(c)] is tentatively placed to feed the $7/2^-$ state based on weak γ-γ coincidences.

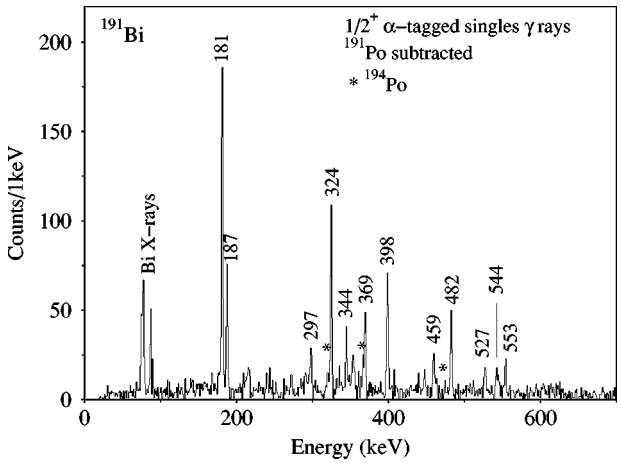

FIG. 13. γ-ray singles spectrum gated by recoils and tagged with the 6870 keV α decay of the $1/2^+$ intruder state in ^{191}Bi. The contaminating γ rays from ^{191}Po have been subtracted and those originating from ^{194}Po are indicated with asterisks.

γ rays feeding the $1/2^+$ intruder state in ^{191}Bi were identified employing the RDT method with a search time of 360 ms to the 6870 keV α decay. However, the focal-plane Si detector with its energy resolution of $\sim$30 keV in this experiment could not separate the 6870 keV α decay from the overlapping lines originating from ^{191}Po and ^{194}Po. The α-decay properties and excited states of ^{191}Po were studied in the present experiment and are reported in Ref. [40]. The half-life of the α-decaying $13/2^+$ state in ^{191}Po is 93(3) ms and the two main decay branches from this state have energies of E_α=7376(5) keV with an intensity of I_α =47.6(1.5)% and E_α=6888(5) keV with I_α=38(8)%. The α-decay energy of ^{194}Po is E_α=6842(6) keV and the half-life 0.392(4)s [41]. In order to distinguish γ rays originating from ^{191}Bi, a background spectrum of γ rays in ^{191}Po correlated with the 7376 keV α decay was generated. Figure 13 shows a spectrum of γ rays tagged with the α decay of the $1/2^+$ state in ^{191}Bi using a search time of 360 ms following the subtraction of the ^{191}Po background spectrum. The lines from the other contaminating isotope ^{194}Po at 320, 367, and 462 keV [11] are just visible.

The 181, 324, 398, and 482 keV transitions are assigned to ^{191}Bi and placed in the level scheme (band 3 in Fig. 12) on the basis of weak γ-γ coincidences and intensity arguments. As the angular distributions of γ rays from low-spin states are expected to be rather isotropic and the statistics is low, an $R_{\rm exp}$ value could only be extracted for the 181 keV γ ray. Even if the obtained value of 0.9(2) for this transition weakly favors a $\Delta I=1$ assignment, the examination of the x rays in the α-tagged spectrum revealed that a 181 keV $M1$ transition would exhaust 80–90 % of the observed x-ray intensity which seems an unrealistically large fraction. Therefore, the γ rays placed to feed the $1/2^+$ state are assumed to be of stretched $E2$ character. The location of the 187, 297, 344, 369, 459, 527, 544, and 553 keV transitions in the level scheme could not be resolved.

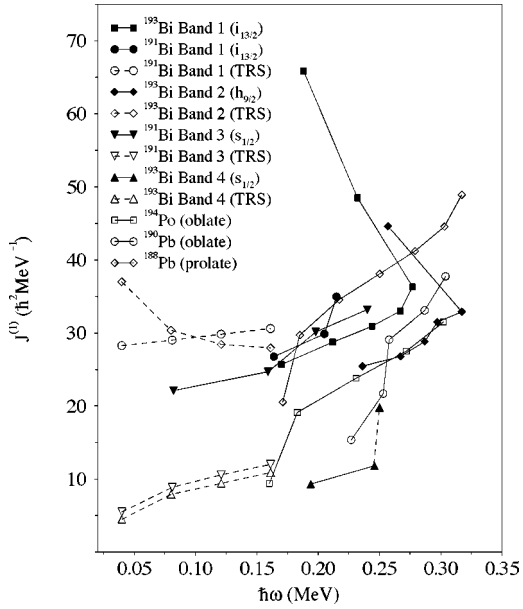

FIG. 14. Experimental kinematic moments of inertia $\mathcal{J}^{(1)}$ for bands 1, 2, and 4 in ^{193}Bi and for bands 1 and 3 in ^{191}Bi (filled symbols). Theoretical predictions from TRS calculations (before neutron alignment) for bands 2 and 4 in ^{193}Bi, for bands 1 and 3 ^{191}Bi (open symbols, dashed line) and experimental values of $\mathcal{J}^{(1)}$ for the yrast bands in ^{194}Po [11] (oblate), ^{190}Pb [8] (oblate), and in ^{188}Pb [42] (prolate) (open symbols, solid line) are also presented. The values for 2^+ states in ^{188,190}Pb are not shown.

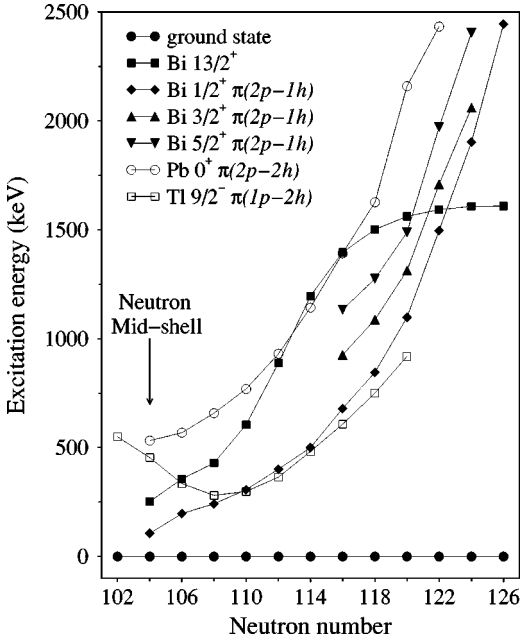

FIG. 15. Systematic behavior of the $1/2^+$, $3/2^+$, and $5/2^+$ intruder [1,14–17,43,44] and the $13/2^+$ isomeric states [13,18,19] in odd-A Bi isotopes with respect to the $9/2^-$ ground state. The excitation energies of the oblate intruder $9/2^-$ states in odd-even Tl [13] and 0^+ states in even-even Pb isotopes (Refs. [13,45], and references therein) with respect to the corresponding ground states are also shown.

IV. DISCUSSION

A. Characteristic states and observed band structures

In recent shell-model calculations, the $9/2^-$ ground states of the odd-A Bi isotopes have been described by a proton in the $h_{9/2}$ orbital interacting with the spherical even-even Pb core. These results indicate a spherical ground state down to ^{193}Bi while the deviation observed in the lighter isotopes is presumably due to the onset of deformation [19]. In the odd-A astatine (Z=85) nuclei, the ground state changes from the spherical $9/2^-$ of the heavier isotopes to the slightly oblate-deformed $1/2^+$ state from the intruder $4p$-$1h$ proton configuration in ^{195}At [14,16]. This change of shape is manifested as a kink in a plot of proton binding energies calculated in the potential of the even-even core, the behavior of which is similar to that observed in the very light odd-A bismuth isotopes.

The low-lying strongly coupled negative-parity bands observed in the present work indicate a deformed configuration involving the odd $h_{9/2}$ proton in both ^{193}Bi and ^{191}Bi. The kinematic moment of inertia $\mathcal{J}^{(1)}$ as a function of rotational frequency for band 2 in ^{193}Bi is plotted in Fig. 14. For comparison, corresponding plots for the oblate bands in ^{190}Pb and ^{194}Po and for the prolate band in ^{188}Pb are also shown. The calculated values of $\mathcal{J}^{(1)}$ for the band in ^{193}Bi are quite similar to those of the band in ^{194}Po, thus suggesting an oblate shape consistently with the performed Woods-Saxon calculations. However, the maximum oblate deformation of $\beta_2 \approx -0.12$ which still preserves the experimentally deduced ground-state spin and parity is not sufficiently large to account for the observed rotational-like level patterns. A natural explanation for such a collective band would be a coupling of the odd proton to the oblate 0^+ $2p$-$2h$ proton excitation of the core instead of the spherical 0^+ configuration.

In the neutron-deficient odd-A Bi isotopes, the isomeric $13/2^+$ state is lowered in excitation energy with decreasing neutron number, as illustrated in Fig. 15 [13,18,19]. Down to ^{195}Bi, this state can be interpreted as a $\pi i_{13/2}$ single-particle state and its behavior partly understood from the $\pi\nu^{-1}$ interaction energies assuming a spherical shape. The interaction of the $i_{13/2}$ proton with holes in the neutron $i_{13/2}$ orbital is less repulsive than that for the $h_{9/2}$ proton thus resulting in the observed trend [20]. The shell-model calculations described in Ref. [19] consider the $13/2^+$ state as an odd proton in the $i_{13/2}$ orbital interacting with the even-even Pb core. This approach well reproduces the behavior of the $13/2^+$ states in the range of $203 \leqslant A \leqslant 209$ while in lighter isotopes, a modification of the $\pi i_{13/2} \otimes \nu f_{5/2}$ interaction strength is necessary. However, the present results for ^{191,193}Bi with collective band structures feeding the $13/2^+$ states stress the importance of deformation in the reduction of the excitation energy. Similarly to the negative-parity band, the most probable configuration of the $13/2^+$ states in these two nuclei would be an $i_{13/2}$ proton coupled to the oblate $2p$-$2h$ 0^+ intruder state of the lead core. The moments of inertia for the $i_{13/2}$ band (band 1) in ^{193}Bi settle between the oblate and prolate configurations of the neighboring nuclei while the corresponding structure in ^{191}Bi shows values slightly closer to the prolate band in ^{188}Pb (Fig. 14).

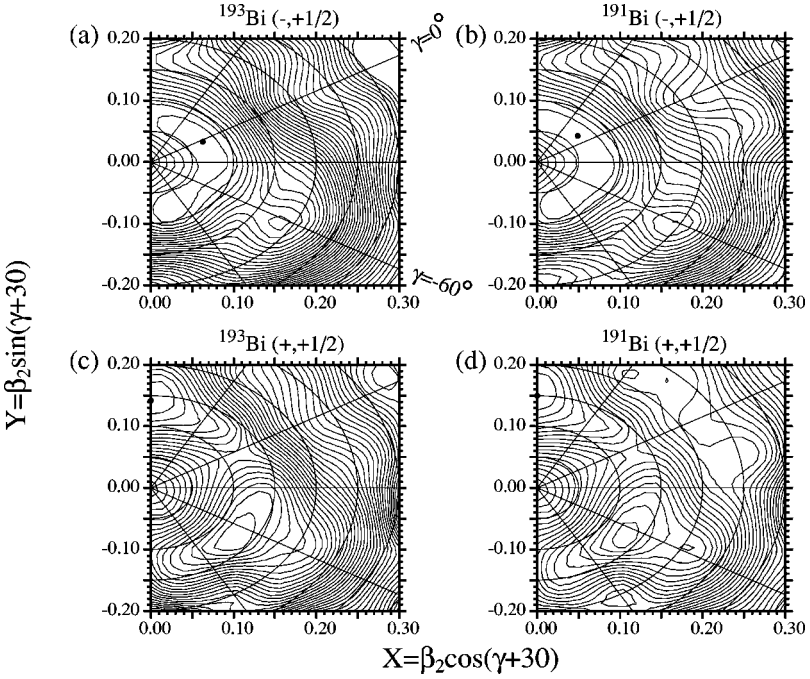

FIG. 16. Total Routhian surfaces at $\hbar\omega = 0.00$ MeV for the $(\pi,\alpha)=(-,+1/2)$ configuration in (a) ^{193}Bi and (b) ^{191}Bi and for the $(\pi,\alpha)=(+,+1/2)$ configuration in (c) ^{193}Bi and (d) ^{191}Bi. The energy difference between the contour lines is 100 keV.

The $1/2^+$ intruder $2p$-$1h$ state from the $s_{1/2}$ orbital is observed down to the last known odd-A isotope ^{185}Bi and low-lying $3/2^+$ and $5/2^+$ intruder states have been established in $^{199-207}$Bi [1,14–17,43,44]. The observed $3/2^+$ and $5/2^+$ states in ^{193}Bi (Fig. 6) and the $5/2^+$ state in ^{191}Bi (Fig. 12) presumably belong to a band based on the $1/2^+$ state. As illustrated in Fig. 15, the excitation energies of the $1/2^+$ states in the heavier isotopes follow a similar parabolic behavior with decreasing N as that found for the oblate $2p$-$2h$ 0_2^+ states in the even-even lead nuclei [13,45]. Close to the $N=104$ midshell, the curve for the Pb isotopes shows signs of leveling off and the $9/2^-$ states from the oblate $1p$-$2h$ configuration in Tl isotopes minimize their energies at $N=108$ [13]. In contrast, the excitation energies of the $1/2^+$ states in the Bi isotopes show a steeper downward trend in going from ^{189}Bi to ^{187}Bi and this state may even become the ground state in ^{185}Bi [44,46,47]. Batchelder *et al.* [48] propose that in the light bismuth isotopes, a prolate $1/2^+$ state instead of the oblate configuration of the heavier isotopes is observed. They also suggest that this state would originate from the $1/2^+[660]$ Nilsson orbital. However, this seems unlikely as the $1/2^+$ member of the high-j band would be pushed higher in excitation energy by the Coriolis interaction. More recent decay studies suggest a gradual change of the observed $1/2^+$ state from an oblate structure in ^{195}Bi via triaxial structures in ^{187,189}Bi to a prolate $1/2^+[400]$ configuration in ^{185}Bi [44].

In the present work, the irregular type of γ-ray spectrum associated with the $1/2^+$ state in ^{193}Bi (Fig. 8) is found to be taken over by a more regular sequence in ^{191}Bi (Fig. 13), indicating some structural change between these two isotopes. The kinematic moments of inertia for the band in ^{193}Bi (band 4) lie well below those for bands associated with oblate shape thus indicating a modest deformation (Fig. 14). In ^{191}Bi, the values of $\mathcal{J}^{(1)}$ for band 3 turn out to be close to those of the prolate band in ^{188}Pb. As the α-decay properties of the observed $1/2^+$ state do not support such a sudden change of configuration, one scenario is that the collective structures would be based on the predicted prolate $1/2^+$ states and the link to the α decaying, dominantly oblate $1/2^+$ configuration remains unobserved.

B. Deformations and intrinsic configurations

1. Negative-parity configurations

Total Routhian surfaces (TRS's) using the Woods-Saxon potential with universal parameters were calculated at several rotational frequencies up to $\hbar\omega=0.40$ MeV for both ^{193}Bi and ^{191}Bi. The plots obtained at $\hbar\omega=0.00$ MeV [Figs. 16(a)–16(d)] reveal the absolute energy minimum in both nuclei to have negative parity and a very small deformation of $\beta_2\approx 0.07$ [marked with a filled circle in Fig. 16(a) and in Fig. 16(b)]. Another negative-parity minimum is located close to the collective oblate axis ($\gamma=-60°$) at $\beta_2\approx 0.18$ and 0.19 in ^{193}Bi and ^{191}Bi, respectively. Even if rotational effects are imposed into the system, these minima remain the main features of the surfaces. In both nuclei, the weakly deformed minimum corresponds to the $9/2^-$ ground state. The observed negative-parity bands are associated with the more-deformed oblate minima which largely involve the proton $2p$-$2h$ excitation from the $s_{1/2}$ orbital across the $Z=82$ shell gap to the $9/2^-[505]$ orbital. Woods-Saxon calculations indicate that the odd proton would occupy the $7/2^-[514]$ state which originates from the $h_{9/2}$ orbital and is mixed with the $7/2^-[503]$ state from the $f_{7/2}$ orbital.

The separation between the weakly deformed and more-deformed oblate minima is calculated to be about 540 keV in ^{193}Bi and decreases to 360 keV in ^{191}Bi. In the present experiments, a candidate for the $7/2^-$ band head in ^{191}Bi was found at 149 keV (Fig. 12) which is a somewhat lower energy than the prediction from the theory. The calculated total energy as a function of spin successfully predicts the cross-

ing of the low-lying oblate and ground-state bands around $I \sim 11/2$. The present results also suggest that the deviation of the binding energy of the ground state compared to the prediction for spherical shape could arise from an oblate component, whose amplitude becomes significant in ^{193}Bi and increases as the neutron number further decreases.

The TRS calculations also yield a theoretical prediction for the kinematic moments of inertia. The calculated values of $\mathcal{J}^{(1)}$ for some of the observed bands as obtained before an alignment of a pair of neutrons in the $i_{13/2}$ orbital are plotted in Fig. 14. The calculations generally rather well reproduce the observed magnitudes while the band-crossing frequencies tend to be lower than those found experimentally, as is the case for the $h_{9/2}$ band in ^{193}Bi.

The observed low-lying bands in the neutron-deficient odd-A Tl isotopes are associated with the coupling of the odd proton in the $h_{9/2}$, $f_{7/2}$, or $i_{13/2}$ orbital to the even-even Hg core (see, for example Ref. [12]). The same proton Nilsson orbitals are situated around the Fermi surface in the odd-A bismuth isotopes and similar configurations can be expected. For strongly coupled bands where the competing $\Delta I=1$ and $\Delta I=2$ transitions are observed, the intrinsic nature of the states can be resolved by examining the probability of the two deexcitation paths as a ratio $B(M1)/B(E2)$. The experimental ratios of reduced transition probabilities [in units $(\mu_N/e\ \mathrm{b})^2$] were extracted using the standard formula

$$\frac{B(M1)}{B(E2)} = 0.697 \frac{E_\gamma^5(I \to I-2) I_\gamma(I \to I-1)}{E_\gamma^3(I \to I-1) I_\gamma(I \to I-2)(1+\delta^2)}, \quad (1)$$

where E_γ is the γ-ray energy (in MeV), I_γ is the γ-ray intensity and δ is the $E2/M1$ mixing ratio. The in-band transitions are assumed to be pure and thus, δ is set to zero. Theoretical $B(M1)/B(E2)$ ratios for bands with various intrinsic configurations can be calculated using the geometrical model [49,50]. The values of g_K for the proton orbitals are obtained from Woods-Saxon calculations and the radius parameter $r_0 = 1.275$ fm has been used in the conversion between Q_0 and β_2 deformation.

The theoretical $B(M1)/B(E2)$ ratios [Fig. 17(c)] for band 2 in ^{193}Bi support the proposed mixed $f_{7/2}/h_{9/2}$ configuration with $\Omega=7/2$ and $g_K=1.16$. Calculations with a pure $h_{9/2}$ structure having $\Omega=9/2$ and $g_K=0.81$ result in unreasonably low values compared to the experiment. The data for the $h_{9/2}$ band in ^{191}Bi are scarce but seem to agree with the calculations when using the same intrinsic configuration as that for the corresponding band in ^{193}Bi [Fig. 17(d)]. This presumed mixed character for this $\Omega=7/2$ Nilsson orbital has also been used to explain the abnormally large strengths of the $11^- \to 8^+$ transitions in the ^{192,190}Pb core nuclei [51].

2. Positive-parity configurations

The positive-parity minimum close to the oblate $\gamma=-60°$ axis at $\beta_2 \approx 0.13$ in both ^{193}Bi [Fig. 16(c)] and ^{191}Bi [Fig. 16(d)] is assigned to the $s_{1/2}$ intruder $2p$-$1h$ proton configuration. Another oblate energy minimum, associated with the high-K $13/2^+[606]$ structure and involving again the proton $2p$-$2h$ excitation lies at $\beta_2 \approx 0.21$ in ^{191}Bi. This minimum is calculated to be located about 700 keV above the

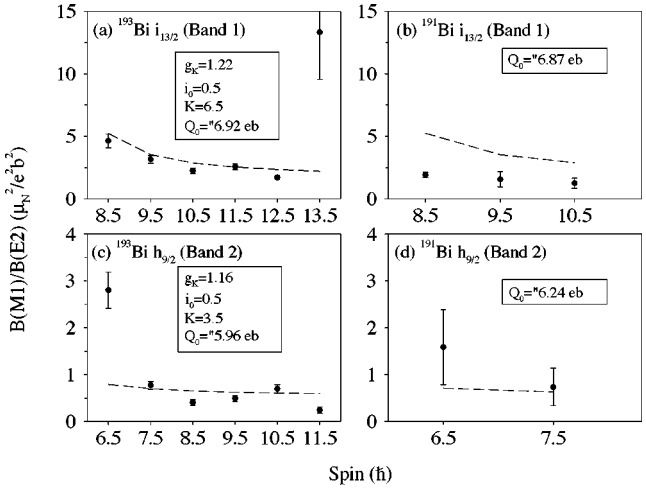

FIG. 17. Experimental $B(M1)/B(E2)$ ratios for bands based on the $13/2^+$ state in (a) ^{193}Bi and (b) ^{191}Bi are marked with filled circles, theoretical estimates are indicated with dashed lines. Corresponding values for bands feeding the $9/2^-$ state are shown for ^{193}Bi in (c) and for ^{191}Bi in (d). The parameter values used for theoretical prediction for each band are indicated for ^{193}Bi, and for ^{191}Bi only if different.

ground state as compared to the 430 keV separation between the $13/2^+$ and $9/2^-$ states found experimentally. In ^{193}Bi, the corresponding structure is not so well distinguished from that at $\beta_2 \approx 0.13$ but develops at higher rotational frequencies. The calculations for ^{191}Bi also reveal triaxial minima which have $\beta_2=0.24-0.27$ ($\gamma=19°$ and $\gamma=-19°$) and are associated with the $1/2^+[660]$ configuration of $\pi i_{13/2}$ origin. In ^{193}Bi, indications of the higher-lying triaxial configuration are observed at larger rotation frequencies.

The prediction of oblate and triaxial, nearly prolate minima from the $i_{13/2}$ proton configuration infers similar structures as those observed in neighboring isotopes. In ^{189}Tl, the oblate and prolate $i_{13/2}$ bands cross between the $17/2^+$ and $21/2^+$ states [52] and similarly, the present calculations for its isotone ^{191}Bi suggest a crossing of the corresponding bands around $I=10$. It remains to be seen in future experiments, whether the 1736 keV level assigned with $I^\pi=(21/2^+)$ (Fig. 12) already belongs to the prolate band. In both ^{187}Tl and ^{185}Tl [12], prolate $i_{13/2}$ bands have been identified down to the $17/2^+$ states, in addition to the beginnings of the oblate bands. In ^{190}Po, the observed yrast band down to the 4^+ state presumably originates from the $6p$-$4h$ intruder configuration giving rise to a prolate deformation [10]. The regular cascade of $E2$ transitions observed in ^{189}Bi has been tentatively interpreted as the prolate $i_{13/2}$ band [25].

The calculated aligned angular momenta for the oblate $i_{13/2}$ band in both ^{191}Bi and ^{193}Bi show an increase of $\sim 14\hbar$ when the rotational frequency is increased from 0.16 to 0.20 MeV, indicating an alignment of a pair of $i_{13/2}$ neutrons. Experimentally, the alignment is found to start at spin 27/2 in ^{193}Bi (Fig. 14) but is not observed in ^{191}Bi where the $i_{13/2}$ band has been established only up to the $21/2^+$ state.

The calculated kinematic moments of inertia for the $i_{13/2}$ band (band 1) in ^{191}Bi qualitatively reproduce the experimental values (Fig. 14). An agreement between the TRS cal-

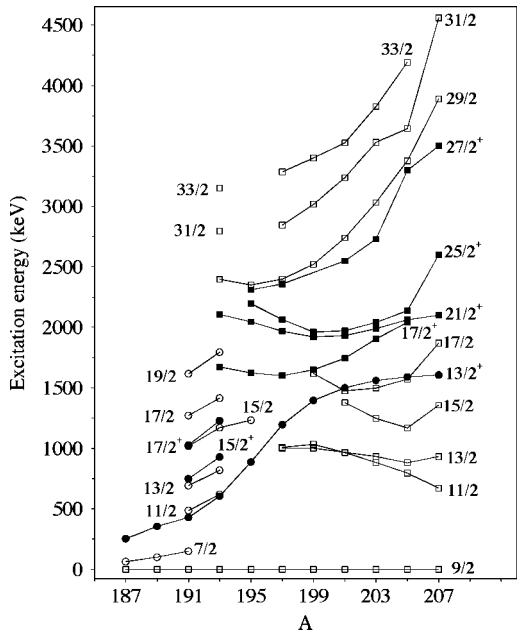

FIG. 18. Systematics of selected low-lying excited states in odd-*A* Bi isotopes. States having positive (negative) parity are marked with filled (open) symbols. Where the exact excitation energy is not known due to unobserved low-energy transitions, Δ is set to 40 keV for clarity. The data are taken from Refs. [53–55] (^{207}Bi), [24,56,57] (^{205}Bi), [23,24,57] (^{203}Bi), [22,58] (^{201}Bi), [22] (^{199}Bi), [21] (^{197}Bi), [20] (^{195}Bi), [16,18] (^{189}Bi), [16,19] (^{187}Bi), and for ^{193,191}Bi from the present work.

culations and experiment is achieved also for the band feeding the $1/2^+$ intruder state in ^{193}Bi. In contrast, the TRS calculations which suggest a similar structure for the $1/2^+$ intruder state in both nuclei, fail to reproduce the observed values of $\mathcal{J}^{(1)}$ for the band feeding this state in ^{191}Bi. The calculations are in accordance with the results of the decay studies which show no abrupt change in the structure of the α-decaying $1/2^+$ state when going from ^{193}Bi to ^{191}Bi [44].

For band 1 in ^{193}Bi, a very good agreement between the experimental $B(M1)/B(E2)$ ratios and the theoretical estimate for an $i_{13/2}$ configuration at the calculated deformation of $\beta_2=-0.21$ is achieved [Fig. 17(a)]. In contrast, the measured ratios for the corresponding structure in ^{191}Bi lie below the theoretical estimate when using similar input parameters [Fig. 17(b)]. One explanation for this behavior could be triaxial shape, an assumption which is supported also by the slightly increased signature splitting in the observed band in ^{191}Bi, as compared to that in ^{193}Bi. In the present calculation, triaxiality would be manifested as a decrease in the effective value of K and indeed, if lower K values are used, the experimental $B(M1)/B(E2)$ ratios can be better reproduced.

C. Cluster interaction approach to ^{193}Bi

The energy systematics of selected low-lying excited states in the odd-*A* bismuth isotopes is presented in Fig. 18. The states in the $i_{13/2}$ and $h_{9/2}$ bands show similar decrease in energy in going from ^{193}Bi to ^{191}Bi, hence supporting the assumption of a similar core configuration for these structures. The deformed states cross the spherical ones in ^{195}Bi and receive most of the population in the lighter isotopes.

Excited states of the heavier odd-*A* Bi isotopes have been successfully interpreted by coupling the odd proton (mainly in the $\pi h_{9/2}$ orbital) to states of the even-even Pb core. This scheme can be expressed as $|\nu J^{\pi},^{A-1}\mathrm{Pb}\rangle \otimes |j_p\rangle = |I^{\pi};^{A}\mathrm{Bi}\rangle$, where ν refers to the core configuration, J^{π} and I^{π} are the total spin and parity of the active state in the Pb and Bi isotones, respectively, and j_p stands for the spin of the odd proton in the bismuth nucleus. In ^{193}Bi, some of the observed states resemble to those in $^{195-201}$Bi [20–22] and a similar approach seems justified. A full shell-model calculation is not tractable but the situation can be simplified by using the net interaction of 16 neutron holes with the odd $h_{9/2}$ proton (see Refs. [21,22]). These so-called cluster interaction energies (E_{cl}) are normalized to the ground-state $(\pi h_{9/2} \otimes \nu 0^+)_{9/2^-}$ interaction which is set at zero. The energies E_{cl} for $^{197-201}$Bi can be extrapolated to the present case and the predictions for the excitation energies of quasiparticle states are obtained by adding up the cluster interaction energies and the excitation energies of the corresponding states in the ^{192}Pb core.

In ^{192}Pb, the low-lying states consist of the fairly regular positive-parity band from 0^+ to 8^+, closely-spaced isomeric 10^+ and 12^+ levels together with the negative-parity 5^-, 7^-, and 9^- states. The ground-state band may be weakly oblate above the 2^+ state and the lowest observed 8^+ state at 2304 keV is interpreted to be a proton intruder whereas the second one at 2520 keV is associated with a neutron configuration [59,60]. The calculated energy levels in ^{193}Bi (E_{theor}) together with the observed states both in ^{192}Pb (E_{core}) and in ^{193}Bi (E_{exp}) are listed in Table III. The negative-parity states of band 2 seem to follow the calculations for the $h_{9/2}$ proton weakly coupled to the 2^+-8^+ states in the ^{192}Pb core. In the heavier isotopes, the positive-parity states are interpreted as the $\pi h_{9/2} \otimes \nu J^-$ configuration, where νJ^- refers to the observed 5^-, 7^-, or 9^- states of the even-even core. The excitation energies of the resulting states, assuming the ground-state proton configuration are also shown in Table III. In ^{193}Bi, the 1672 keV $(17/2^+)$ and either one of the 2108 and 2127 keV levels closely follow the systematics of the $17/2^+$ and $21/2^+$ states of $h_{9/2} \otimes 5^-$ and $h_{9/2} \otimes 7^-$ parentage, respectively. Hence, these states presumably correspond to those observed in ^{195}Bi where they are yrast.

D. Isomeric states

The properties of the isomeric states, observed in the present work via γ-ray detection in ^{193}Bi and in ^{191}Bi are compiled in Table IV. Apart from the low-lying $13/2^+$ states, evidence for two high-spin isomers was found in ^{193}Bi and indications of one in ^{191}Bi. In addition, the missing link between group B and the rest of the level scheme (Fig. 6) may infer still another isomeric state in ^{193}Bi. Since the direct deexcitations of these states were not observed, their excitation energies and spins could not be determined. However, isomeric $29/2^-$ states have been established in the heavier odd-*A* bismuth isotopes and the systematics suggests such a state at around 2.4 MeV in excitation energy in ^{193}Bi (Fig.

TABLE III. Predicted excitation energies (E_{theor}) of states (I^{π}) in ^{193}Bi, calculated as the coupling of the odd proton (j_p) to the state in ^{192}Pb core ($\nu J^{\pi}, E_{\text{core}}$) using the cluster interaction approach. The experimental energies obtained in the present work for ^{193}Bi (E_{exp}) are also given. All energies are in units keV.

νJ^{π}	E_{core}	j_p	I^{π}	E_{theor}	E_{exp}
2^+	854	$h_{9/2}$	$11/2^-$	850	620
		$h_{9/2}$	$13/2^-$	750	818
4^+	1356	$h_{9/2}$	$15/2^-$	1220	1170
		$h_{9/2}$	$17/2^-$	1280	1415
5^-	1860	$h_{9/2}$	$17/2^+$	1660	1672
6^+	1921	$h_{9/2}$	$19/2^-$		1795
		$h_{9/2}$	$21/2^-$		2050
7^-	2323	$h_{9/2}$	$21/2^+$	2100	2108 or 2127
9^-	2514	$h_{9/2}$	$25/2^+$	2400	
		$h_{9/2}$	$27/2^+$	2400	
8^+	2520	$h_{9/2}$	$23/2^-$		2464
		$h_{9/2}$	$25/2^-$		2588
12^+	2625	$h_{9/2}$	$29/2^-$	2420	2400[a]
		$h_{9/2}$	$31/2^-$	2925	2800[a]
		$h_{9/2}$	$33/2^-$	3300	3150[a]

[a]The presumed unobserved $(29/2^-) \rightarrow (25/2^-)$ transition energy is set to 40 keV.

18, Table III). This agrees with the energy of the 3 μs isomer, provided that energy of the unobserved deexciting transition is below the detection limit in the present experiment. The isomeric $(29/2^-)$ state together with the $(31/2^-)$ and $(33/2^-)$ states are interpreted to be of the $\pi h_{9/2} \otimes \nu i_{13/2}^{-2}$ configuration, in good agreement with the cluster interaction calculations (Table III).

In ^{195}Bi the isomeric $(29/2)^-$ state ($t_{1/2}$=750 ns) deexcites to a $(27/2^+)$ state and consecutively to a $(25/2^+)$ and $(21/2^+)$ state by low-energy transitions [20]. In ^{193}Bi, the topmost state below the 3-μs isomer is assigned to have a spin and parity of $I^{\pi}=(25/2^-)$ which suggests a change in the decay path as compared to ^{195}Bi. If the deexcitation of the isomeric state in ^{193}Bi proceeds via a single transition to the $(25/2^-)$ state, the corresponding isomeric transition in the core would be $h_{9/2} \otimes 12^+ \rightarrow h_{9/2} \otimes 10^+$. In $A \sim 190$ lead nuclei, the transition between the 12^+ and 10^+ states from the neutron $i_{13/2}^2$ configuration is hindered due to the fact that the neutron $i_{13/2}$ orbital is half-filled [61,62].

TABLE IV. Properties of isomeric levels in ^{191,193}Bi.

Nucleus	Level energy (keV)	I^{π}	$t_{1/2}$
^{191}Bi	430	$13/2^+$	562(10) ns
^{191}Bi			400(40) ns
^{193}Bi	605	$13/2^+$	153(10) ns
^{193}Bi	$2357+\Delta$	$(29/2^-)$	3.0(1) μs
^{193}Bi			>10 μs

The other isomer in ^{193}Bi with a halflife of $t_{1/2}>10$ μs is probably located just above the 2108 and 2127 keV levels and is much more difficult to interpret. Although many isomeric states have been observed in the heavier bismuth isotopes, none of these is as long lived. As illustrated in Fig. 18, the energy difference between the $27/2^+$ and $25/2^+$ states presumably of $h_{9/2} \otimes 9^-$ origin significantly decreases when going from ^{197}Bi to ^{195}Bi. This suggests that in ^{193}Bi, the $27/2^+$ state may be located below the $25/2^+$ state hence resulting in an relatively long-lived isomeric state. Another possibility is that this structure would relate to the 11^- isomeric states which are associated with the oblate $\pi(i_{13/2} \otimes h_{9/2})$ configuration in Pb [8] and Po [63] nuclei. A weakly oblate band with a $\pi(i_{13/2} \otimes h_{9/2}^2)$ character in ^{193}Bi would have $K=29/2$ and the band head might be isomeric. In both cases, the isomeric state would deexcite via some intermediate state(s) to the observed 2108 and 2127 keV levels.

V. SUMMARY

The very neutron-deficient ^{191,193}Bi nuclei have been studied at the gas-filled recoil separator RITU by using Ge-detector arrays for the observation of both prompt and delayed γ rays. Prior to the present work, only the α-decaying $9/2^-$ ground and $1/2^+$ intruder states were known in these two isotopes. Using the selective recoil-decay tagging (RDT), recoil gating, and isomer tagging analysis techniques, excited states in ^{191}Bi and ^{193}Bi have for the first time been identified and extensive level schemes for both nuclei have been constructed. The level structures now observed disclose the competition between various nuclear shapes in the light bismuth isotopes close to the $82<N<126$ midshell.

The isomeric $13/2^+$ states were established in both ^{191}Bi and ^{193}Bi and associated strongly coupled oblate-deformed bands were observed. A negative-parity band feeding the $9/2^-$ ground state, also having properties consistent with an oblate-deformed structure above the ground state, was observed in both nuclei. The intrinsic excitation of this band is assumed to be a mixed $h_{9/2}/f_{7/2}$ configuration with $\Omega=7/2$. Quasiparticle states corresponding to spherical structures of the heavier odd-A isotopes were observed in ^{193}Bi. Bands feeding the α-decaying $1/2^+$ states were identified and their properties indicate some structural change between the ^{193}Bi and ^{191}Bi isotopes. Two higher-lying isomers, having halflives of $t_{1/2}=3$ μs and $t_{1/2}>10$ μs were observed in ^{193}Bi, the former continuing the systematic trend of isomeric $29/2^-$ states from the $h_{9/2} \otimes 12^+$ configuration. In ^{191}Bi, indications of an isomeric state with a halflife of $t_{1/2}=400$ ns were obtained.

Nuclear shapes associated with various structures in ^{191}Bi and ^{193}Bi were extracted from TRS calculations. These calculations predict a nearly spherical $9/2^-$ ground state for both isotopes and deformations of $\beta_2=0.21$ and $\beta_2=0.18-0.19$ for the oblate $i_{13/2}$ and $h_{9/2}/f_{7/2}$ configurations, respectively. Both structures involve the proton $2p$-$2h$ intruder excitation across the $Z=82$ shell gap. The calculated potential

surfaces for positive-parity configurations also reveal minima at a more-deformed nearly prolate shape which are associated with the proton $1/2^+[660]$ configuration and in ^{191}Bi, a candidate band member for this low-Ω $i_{13/2}$ structure is found. For the intruder $s_{1/2}$ configuration, a deformation of $\beta_2 = 0.13$ in both nuclei is predicted, being consistent with the observed level pattern in ^{193}Bi, while that of ^{191}Bi indicates increased collectivity. One explanation for this change could be the coexistence of two $1/2^+$ states, the other being the band head of a prolate band while the other would be the α-decaying oblate $2p$-$1h$ configuration. However, this scenario could not be confirmed from the present data.

ACKNOWLEDGMENTS

This work has been supported by the Academy of Finland under the Finnish Centre of Excellence Programme 2000-2005 (Project No. 44875, Nuclear and Condensed Matter Programme at JYFL) and by the European Union Fifth Framework Programme "Improving Human Potential - Access to Research Infrastructure."

[1] K. Heyde, P. Van Isacker, M. Waroquier, J. L. Wood, and R. A. Meyer, Phys. Rep. **102**, 291 (1983).
[2] J. L. Wood, K. Heyde, W. Nazarewicz, M. Huyse, and P. Van Duppen, Phys. Rep. **215**, 101 (1992).
[3] S. Frauendorf and V. V. Paskevich, Phys. Lett. **55B**, 365 (1975).
[4] J. Bonn, G. Huber, H.-J. Kluge, and E. W. Otten, Z. Phys. A **276**, 203 (1976).
[5] S. Nilsson, K. Dan. Vidensk. Selsk. Mat. Fys. Medd. **29**(16), 1 (1955).
[6] K. Heyde, J. Ryckebusch, M. Waroquier, and J. L. Wood, Nucl. Phys. **A484**, 275 (1988).
[7] R. Julin, K. Helariutta, and M. Muikku, J. Phys. G **27**, R109 (2001).
[8] G. D. Dracoulis, A. P. Byrne, and A. M. Baxter, Phys. Lett. B **432**, 37 (1998).
[9] D. G. Jenkins *et al.*, Phys. Rev. C **62**, 021302(R) (2000).
[10] K. Van de Vel *et al.*, Eur. Phys. J. A **17**, 167 (2003).
[11] K. Helariutta *et al.*, Eur. Phys. J. A **6**, 289 (1999).
[12] G. J. Lane, G. D. Dracoulis, A. P. Byrne, P. M. Walker, A. M. Baxter, J. A. Sheikh, and W. Nazarewicz, Nucl. Phys. **A586**, 316 (1995).
[13] *Table of Isotopes*, edited by R. B. Firestone, V. S. Shirley, S. Y. F. Chu, C. M. Baglin, and J. Zipkin, 8th ed. (Wiley, New York, 1996), Vol. II.
[14] H. Kettunen *et al.*, Eur. Phys. J. A **16**, 457 (2003).
[15] E. Coenen, K. Deneffe, M. Huyse, P. Van Duppen, and J. L. Wood, Phys. Rev. Lett. **54**, 1783 (1985).
[16] H. Kettunen *et al.*, Eur. Phys. J. A **17**, 537 (2003).
[17] M. Alpsten and G. Astner, Nucl. Phys. **A134**, 407 (1969).
[18] A. N. Andreyev *et al.*, Eur. Phys. J. A **10**, 129 (2001).
[19] A. Hürstel *et al.*, Eur. Phys. J. A **15**, 329 (2002).
[20] T. Lönnroth, C. W. Beausang, D. B. Fossan, L. Hildingsson, W. F. Piel, Jr., M. A. Quader, S. Vajda, T. Chapuran, and E. K. Warburton, Phys. Rev. C **33**, 1641 (1986).
[21] T. Chapuran, K. Dybdal, D. B. Fossan, T. Lönnroth, W. F. Piel, Jr., D. Horn, and E. K. Warburton, Phys. Rev. C **33**, 130 (1986).
[22] W. F. Piel, Jr., T. Chapuran, K. Dybdal, D. B. Fossan, T. Lönnroth, D. Horn, and E. K. Warburton, Phys. Rev. C **31**, 2087 (1985).
[23] H. Hübel, A. Kleinrahm, C. Günther, D. Mertin, and R. Tischler, Nucl. Phys. **A294**, 177 (1978).
[24] T. Lönnroth, Z. Phys. A **307**, 175 (1982).
[25] A. Hürstel *et al.* (unpublished).
[26] P. Nieminen *et al.*, Acta Phys. Pol. B **32**, 1019 (2001).
[27] P. Nieminen *et al.*, in *Proceedings of the Conference on Frontiers of Nuclear Structure*, edited by P. Fallon and R. Clark, AIP Conf. Proc. No. 656 (AIP, Melville, 2003), p. 63.
[28] C. W. Beausang *et al.*, Nucl. Instrum. Methods Phys. Res. A **313**, 37 (1992).
[29] M. Moszyński, J. H. Bjerregard, J. J. Gaardhoje, B. Herskind, P. Knudsen, and G. Sletten, Nucl. Instrum. Methods Phys. Res. A **280**, 73 (1989).
[30] P. J. Nolan, D. W. Gifford, and P. J. Twin, Nucl. Instrum. Methods Phys. Res. A **236**, 95 (1985).
[31] M. Leino *et al.*, Nucl. Instrum. Methods Phys. Res. B **99**, 653 (1995).
[32] H. Kettunen *et al.*, in *Proceedings of Conference Proton-Emitting Nuclei, Second International Symposium PROCON 2003*, edited by E. Maglione and F. Soramel, AIP Conf. Proc. No. 681 (AIP, Melville, 2003), p. 26.
[33] R. S. Simon, K.-H. Schmidt, F. P. Hessberger, S. Hlavac, M. Honusek, G. Münzenberg, H.-G. Clerc, U. Gollerthan, and W. Schwab, Z. Phys. A **325**, 197 (1986).
[34] E. S. Paul *et al.*, Phys. Rev. C **51**, 78 (1995).
[35] A. Artna-Cohen, Nucl. Data Sheets **83**, 921 (1998).
[36] M. B. Smith *et al.*, Eur. Phys. J. A **5**, 43 (1999).
[37] D. C. Radford, Nucl. Instrum. Methods Phys. Res. A **361**, 297 (1995).
[38] J. M. Lagrange, M. Pautrat, J. S. Dionisio, C. Vieu, and J. Vanhorenbeeck, Nucl. Phys. **A530**, 437 (1991).
[39] F. Rösel, H. M. Fries, K. Alder, and H. Pauli, At. Data Nucl. Data Tables **21**, 291 (1978).
[40] A. N. Andreyev *et al.*, Phys. Rev. C **66**, 014313 (2002).
[41] J. Wauters, P. Dendooven, M. Huyse, G. Reusen, P. Van Duppen, P. Lievens, and the ISOLDE Collaboration, Phys. Rev. C **47**, 1447 (1993).
[42] J. Heese, K. H. Maier, H. Grawe, J. Grebosz, H. Kluge, W. Meszynski, M. Schramm, R. Schubart, K. Spohr, and J. Styczen, Phys. Lett. B **302**, 390 (1993).
[43] R. A. Braga, W. R. Western, J. L. Wood, R. W. Fink, R. Stone, C. R. Bingham, and L. L. Riedinger, Nucl. Phys. **A349**, 61 (1980).
[44] A. N. Andreyev *et al.*, Phys. Rev. C **69**, 054308 (2004).
[45] K. Van de Vel *et al.*, Phys. Rev. C **65**, 064301 (2002).
[46] C. N. Davids *et al.*, Phys. Rev. Lett. **76**, 592 (1996).
[47] G. L. Poli *et al.*, Phys. Rev. C **63**, 044304 (2001).

[48] J. C. Batchelder *et al.*, Eur. Phys. J. A **5**, 49 (1999).
[49] F. Dönau and S. Frauendorf, in *Proceedings of the Conference on High Angular Momentum Properties of Nuclei*, Oak Ridge, 1982, edited by N. Johnson (Harwood, New York, 1983), p. 143.
[50] F. Dönau, Nucl. Phys. **A471**, 469 (1987).
[51] G. D. Dracoulis, T. Kibedi, A. P. Byrne, A. M. Baxter, S. M. Mullins, and R. A. Bark, Phys. Rev. C **63**, 061302(R) (2001).
[52] A. J. Kreiner, J. Davidson, M. Davidson, H. Mosca, L. L. Riedinger, C. R. Bingham, M. W. Guidry, and A. C. Kahler, Phys. Rev. C **38**, 2674 (1988).
[53] I. Bergström, C. J. Herrlander, P. Thieberger, and J. Blomqvist, Phys. Rev. **181**, 1642 (1969).
[54] T. Lönnroth and B. Fant, Phys. Scr. **18**, 172 (1978).
[55] T. Lönnroth, J. Blomqvist, I. Bergström, and B. Fant, Phys. Scr. **19**, 233 (1979).
[56] R. Brock, C. Günther, H. Hübel, A. Kleinrahm, D. Mertin, P. Meyer, and R. Tischler, Nucl. Phys. **A278**, 45 (1977).
[57] H. Hübel, M. Guttormsen, K. P. Blume, J. Recht, A. von Grumbkow, K. Hardt, P. Schüler, Y. Agarwal, and A. Maj, Z. Phys. A **314**, 89 (1983).
[58] R. Broda, C. Günther, and B. V. Thirumala Rao, Nucl. Phys. **A389**, 366 (1982).
[59] C. M. Baglin, Nucl. Data Sheets **84**, 717 (1998).
[60] A. J. M. Plompen *et al.*, Nucl. Phys. **A562**, 61 (1993).
[61] R. Broda *et al.*, Phys. Rev. Lett. **68**, 1671 (1992).
[62] J. J. Van Ruyven, J. Penninga, W. H. A. Hesselink, P. Van Nes, K. Allaart, E. J. Hengeveld, H. Verheul, M. J. A. De Voigt, Z. Sujkowski, and J. Blomqvist, Nucl. Phys. **A449**, 579 (1986).
[63] A. Maj, H. Grave, H. Kluge, A. Kuhnert, K. H. Maier, J. Recht, N. Roy, H. Hübel, and M. Guttormsen, Nucl. Phys. **A509**, 413 (1990).